

Exploring the Adjugate Matrix Approach to Quaternion Pose Extraction

Andrew J. Hanson
Indiana University
Bloomington, IN
hansonaj@indiana.edu

Sonya M. Hanson
The Flatiron Institute
New York, NY
shanson@flatironinstitute.org

February 11, 2023

Abstract

Quaternions are important for a wide variety of rotation-related problems in computer graphics, machine vision, and robotics. We study the nontrivial geometry of the relationship between quaternions and rotation matrices by exploiting the adjugate matrix of the characteristic equation of a related eigenvalue problem to obtain the manifold of the space of a quaternion eigenvector. We argue that quaternions parameterized by their corresponding rotation matrices cannot be expressed, for example, in machine learning tasks, as single-valued functions: the quaternion solution must instead be treated as a manifold, with different algebraic solutions for each of several single-valued sectors represented by the adjugate matrix. We conclude with novel constructions exploiting the quaternion adjugate variables to revisit several classic pose estimation applications: 2D point-cloud matching, 2D point-cloud-to-projection matching, 3D point-cloud matching, 3D orthographic point-cloud-to-projection matching, and 3D perspective point-cloud-to-projection matching. We find an exact solution to the 3D orthographic least squares pose extraction problem, and apply it successfully also to the perspective pose extraction problem with results that improve on existing methods.

1 Introduction

We address the task of understanding whether there are obstacles to using quaternions to represent orientation space, typical examples being the determination of the optimal rotation to align two matched 2D or 3D point clouds, or find the pose of the 2D or 3D point cloud that produced a given projected image; see Fig. (1). Our approach is to carefully study how to compute the optimal quaternion corresponding to a given measurement of a (typically inexact) rotation matrix.

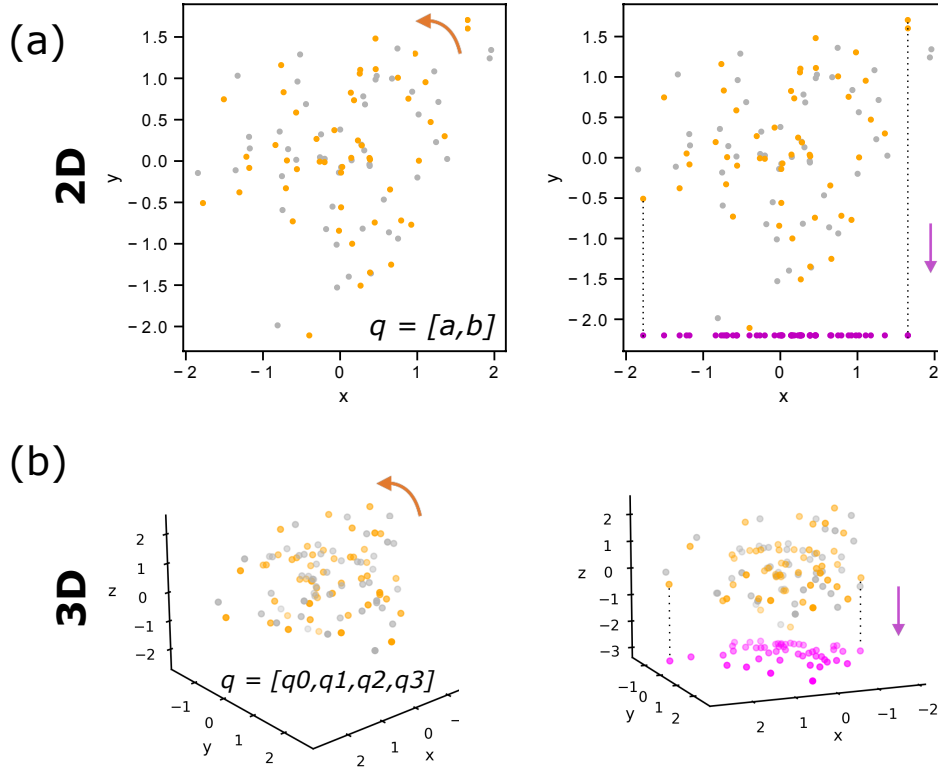


Figure 1: **The fundamental point-cloud matching problems in 2D and 3D.** Grey points indicate a reference point-cloud, orange points indicate a rotated point-cloud, and magenta points are projections. In this paper rotations are represented by quaternion rotation parameters: $q = [a, b]$ for 2D rotations and $q = [q_0, q_1, q_2, q_3]$ for 3D rotations. (a) Left: Alignment between a 2D reference cloud and a 2D test cloud differing by a rotation. Right: Alignment between a 2D reference cloud and a rotated cloud producing a 1D projected image. (b) Left: Alignment between a 3D reference cloud and a 3D test cloud differing by a rotation. Right: Alignment between a 3D reference cloud and a rotated cloud producing a 2D projected image.

The optimal-quaternion extraction problem is universal, and occurs in many frameworks, reflecting the appealing fact that unit quaternions form a smooth manifold that parameterizes rotations free of Euler angle issues such as gimbal lock (see, e.g. Hanson (2006, 2020)). Our investigation is motivated particularly by what has been referred to as the “quaternion discontinuity problem” in the context of machine learning in rotation space by, e.g., Saxena et al. (2009); Zhou et al. (2019); Peretroukhin et al. (2020); Zhao et al. (2020); Xiang and Li (2020). Understanding such potential issues is important, as the determination of orientation and pose is widespread in machine learning applications, including self-driving vehicles, drone navigation, and general problems of understanding 3D space, evaluating 3D

models, and the extraction of 3D information from 2D data.

Our first contribution is to show explicitly how the topological properties of a quaternion, understood as a multi-sector manifold, resolve the questions regarding discontinuities posed in certain sectors of the machine learning literature. Traditional computational algorithms (see, e.g., Shepperd (1978); Sarabandi and Thomas (2019); Hanson (2006)) for extracting a corresponding quaternion from a 3D rotation matrix have always included specific methods to account for possible singularities and discontinuities in the mapping, but have not been clearly incorporated into some of the recent literature in which such issues have been encountered. We show how to exploit a classic linear algebra construction known formally as the *adjugate matrix*; remarkably, the adjugate embodies an alternative set of quaternion-related variables that has surprising use cases, greatly clarifies how the traditional quaternion extraction algorithms avoid singularities, and enables the exact solution of certain challenging pose-estimation problems. The adjugate suggests a new appreciation of the variational method for quaternion extraction introduced by Bar-Itzhack (2000), and enables unique ways of applying least squares methods to solve 3D rotation discovery problems. In particular, we can use the adjugate variables to find a closed-form formula solving a least squares optimization formula for pose estimation. We are thus able to explain the origin and resolution of the discontinuity problem, and to further exploit our technology to provide novel insights into pose estimation.

Outline: In the following, we illustrate our arguments beginning with a simplified and intuitive 2D rotation framework that exhibits essentially all the relevant properties. We explore three ways of looking at the 2D problem in preparation for a parallel treatment of the application-relevant 3D quaternion-rotation case: we begin by considering 2D rotations as special cases of 3D rotations to produce a pair of formulas for the 2×2 orthonormal 2D rotation matrix. We gain new insights by solving these for the 2D quaternion variables directly. We then explore the 2D version of a variational method due to Bar-Itzhack (2000), minimizing a difference measure between the two relevant matrices. Next, we replace the ideal, error-free 2D rotation matrix by a noisy version for which each matrix element is still close to a rotation matrix element, but is treated algebraically as distinct. The variational methods expose in further detail how to understand the multivalued nature of the 2D quaternion extraction problem. We repeat a similar analysis to derive the corresponding 3D results, determining how to extract complete quaternion information without singularities or discontinuities from 3D rotation matrices, for both ideal and noisy data elements. Finally, we study some applications of the adjugate variables as parameters replacing the quaternions themselves in rotation optimization applications, and show in particular how the problem of estimating the pose in 3D space of a 2D point image relative to its corresponding 3D point cloud can be computed in closed form using only rational polynomials combined with a Bar-Itzhack optimization.

2 Fundamental Background

The arguments we present in this paper rely on a short list of key background concepts. Our description of the problem at hand relies on the relationship between two ways of representing a rotation matrix. Furthermore, error-robust quaternion extraction can be done in two basic ways. These four concepts are described below:

Representing rotations:

- **Quaternions parameterize a rotation in terms of a point on a topological three-sphere.** Any 4D vector q with unit length¹, $q \cdot q = 1$, is a quaternion point on the unit three-sphere \mathbf{S}^3 , and corresponds exactly to a *proper* 3D rotation matrix $R = R(q)$ through the equation

$$R(q) = \begin{bmatrix} q_0^2 + q_1^2 - q_2^2 - q_3^2 & 2q_1q_2 - 2q_0q_3 & 2q_1q_3 + 2q_0q_2 \\ 2q_1q_2 + 2q_0q_3 & q_0^2 - q_1^2 + q_2^2 - q_3^2 & 2q_2q_3 - 2q_0q_1 \\ 2q_1q_3 - 2q_0q_2 & 2q_2q_3 + 2q_0q_1 & q_0^2 - q_1^2 - q_2^2 + q_3^2 \end{bmatrix}. \quad (1)$$

This fundamental equation is quadratic in q , so $R(q) = R(-q)$, and thus every possible rotation is represented *twice* in the manifold \mathbf{S}^3 . Alternatively, one can say that every possible rotation appears *once* in a hyperhemisphere of \mathbf{S}^3 , the solid three-ball \mathbf{B}^3 that can be drawn in ordinary 3D space. In mathematical terms, Eq. (1) can also be described in terms of the group $\mathbf{SO}(3)$, whose topological manifold is \mathbf{RP}^3 , the real projective 3-space, but we will not need to consider that feature in our treatment.

- **Quaternions encompass the axis-angle rotation parameterization.** The axis-angle representation $R = R(\theta, \hat{\mathbf{n}})$ parameterizes any 3D rotation in terms of the unit eigenvector $\hat{\mathbf{n}}$ of R , the direction fixed by the rotation, and the angle θ of that rotation. With $c = \cos \theta$ and $s = \sin \theta$, any rotation matrix can be written explicitly using axis-angle parameters as

$$R(\theta, \hat{\mathbf{n}}) = \begin{bmatrix} c + (1-c)\hat{n}_1^2 & (1-c)\hat{n}_1\hat{n}_2 - s\hat{n}_3 & (1-c)\hat{n}_1\hat{n}_3 + s\hat{n}_2 \\ (1-c)\hat{n}_1\hat{n}_2 + s\hat{n}_3 & c + (1-c)\hat{n}_2^2 & (1-c)\hat{n}_2\hat{n}_3 - s\hat{n}_1 \\ (1-c)\hat{n}_1\hat{n}_3 - s\hat{n}_2 & (1-c)\hat{n}_2\hat{n}_3 + s\hat{n}_1 & c + (1-c)\hat{n}_3^2 \end{bmatrix}. \quad (2)$$

Choosing the quaternion parameterization

$$q(\theta, \hat{\mathbf{n}}) = (\cos(\theta/2), \sin(\theta/2)\hat{\mathbf{n}}) \quad (3)$$

and substituting it into Eq. (1) gives exactly Eq. (2), double covered with $0 \leq \theta < 4\pi$.

¹Henceforth, we will always be assuming unit-length quaternions.

Error-robust quaternion extraction:

- **Classical error-robust quaternion extraction is hard.** The rotation matrices described in Eq. (1) and Eq. (2) are exact. However, extracting the optimal quaternion representation of an inexact measured rotation matrix $R(m)$, with measured numerical matrix elements m_{ij} , is not an exact procedure. The task can be defined as the problem of recovering the best axis-angle parameters describing $R(m)$. This is well-known to be a subtle multi-step process (see, e.g., Shepperd, 1978; Hanson, 2006; Sarabandi and Thomas, 2019). In order to account for all possible anomalies, however rare, the classical procedure must check for zeros, conducting several separate checks for small numbers (see Appendix A for detailed pseudocode and examples). This algorithm reliably generates the axis-angle parameters $\cos \theta$, $\sin \theta$, and $\hat{\mathbf{n}}$ needed to define a provably optimal $q(\theta, \hat{\mathbf{n}})$ from the numerical data in $R(m)$. Note that this procedure assumes $R(m)$ is perfectly described by Eq. (2), and thus does not gracefully handle finding the quaternion that is the best approximation for an imperfectly measured $R(m)$; this can be achieved using the variational method of Bar-Itzhack (2000), which will play a significant role in our narrative.
- **The adjugate matrix approach to eigenvectors is important.** A standard method for finding the optimal quaternion corresponding to a rotation aligning two 3D point clouds uses the quaternion eigenvector corresponding to the maximal eigenvalue of the 4×4 *profile matrix* M (see, e.g., Horn, 1987; Hanson, 2020). In our treatment we will take advantage of a construction called the ‘adjugate’. (Further details may be found in Appendix C.) The adjugate of any square matrix S is built from the matrix’s transposed cofactors, which facilitate the construction of the inverse through the following identity:

$$S \cdot \text{Adjugate}(S) = \det S \, I_4 . \quad (4)$$

To see how this is exploited, we consider the characteristic matrix of M

$$\chi = [M - \lambda I_4] , \quad (5)$$

whose characteristic equation $\det \chi = 0$, quartic in λ , determines the eigenvalues of M . We then insert the maximal eigenvalue λ_{opt} into the matrix, setting $\chi = \chi(\lambda_{\text{opt}})$, and multiply that characteristic matrix by its adjugate as follows:

$$\chi \cdot \text{Adjugate}(\chi) = \det \chi \, I_4 = 0 . \quad (6)$$

This allows us, via Eq. (5), to write the solved eigensystem of M as

$$M \cdot \text{Adjugate}(\chi) - \lambda_{\text{opt}} \text{Adjugate}(\chi) = 0 . \quad (7)$$

We see that each of the adjugate’s four column vectors is an eigenvector of the single eigenvalue λ_{opt} ; thus the adjugate provides *four* parallel solutions to the same

eigensystem, and hence embodies four apparently equivalent unnormalized optimal quaternions q_{opt} .

Starting from this list of observations, we will use the relationships between quaternions and rotation matrices to show there are no singularity-free single functions relating a quaternion to a measured rotation matrix, but that an adjugate matrix, listing four alternatives (technically eight, taking into account the quaternion sign ambiguity) describing the entire quaternion manifold \mathbf{S}^3 , always contains at least one normalizable column that produces a valid quaternion.

3 Two-Dimensional Rotations and the Quaternion Map

While quaternions are the most robust possible representation of rotations, computing the relationship between a rotation matrix and a quaternion exposes unexpected singularities. The singularities we wish to investigate occur already for 2D rotations and their quaternion counterparts, so we begin our journey in the simpler 2D space. The context in the back of our minds is the exploration of data sets of (reference, sample) pairs of matched ND point clouds (r, s) related by a single rotation matrix R ,

$$s = R \cdot r + \langle \text{noise} \rangle ,$$

or

$$s = R \cdot (r + \langle \text{noise} \rangle) ,$$

depending on how one views the application context. We will resolve apparent discrepancies in the use of quaternions to solve such problems first in 2D by introducing the adjugate variables.

3.1 Direct Solution of the Two-Dimensional Problem

We begin with the simplified context of 2D rotations, obtained by setting $q_1 = q_2 = 0$ and $\hat{n}_1 = \hat{n}_2 = 0$ in Eqs. (1) and (2) to restrict rotations to the (x, y) plane, that is, fixing the \hat{z} axis. For convenience, we define $c = \cos \theta$, $s = \sin \theta$, $a = q_0 = \cos(\theta/2)$, and $b = q_3 = \sin(\theta/2)$, so $c^2 + s^2 = a^2 + b^2 = 1$. We observe that, taking the range $0^\circ \leq \theta < 720^\circ$, a and b cover the (a, b) circle only once, while the (c, s) pair covers its circle twice over this range. With these parameterizations, we can now construct ideal algebraic forms of either a

quaternion-parameterized 2D rotation matrix or a standard 2D rotation matrix as follows:

$$R(a, b) = \begin{bmatrix} a^2 - b^2 & -2ab \\ 2ab & a^2 - b^2 \end{bmatrix} \quad (8)$$

$$R(c, s) = \begin{bmatrix} c & -s \\ s & c \end{bmatrix} . \quad (9)$$

We easily verify that $\det R(a, b) = \det R(c, s) = 1$, and also that $R \cdot R^t = I_2$, where I_2 is the 2D identity matrix. The most important property of $R(c, s)$ is that its matrix elements correspond to a *numerically measurable* rotation matrix, as do noisy versions of $R(c, s)$, which we will distinguish by the notation $R(m)$ for separate treatment, while we will see that $R(a, b)$ has some intriguing ambiguities.

Now suppose we erase the formulas for R in terms of θ , and think only of the algebraic expressions in Eqs. (8, 9), assuming that we have some sound way of measuring this 2D rotation to determine the numerical values of (c, s) . Then we can find expressions for the now-abstract variables (a, b) in several ways. We begin by noting that both constraints $R(a, b) = R(c, s)$ and $R(a, b) \cdot R(c, s)^t = I_2$ produce the same equations,

$$\begin{aligned} a^2 - b^2 &= c \\ 2ab &= s , \end{aligned} \quad (10)$$

which are simply the trigonometric half-angle formulas. We now take an important step: assuming the constraint $a^2 + b^2 = 1$, we can eliminate either a^2 or b^2 , and complete our solution in terms of the measured rotation transformation parameters (c, s) in two very distinct ways:

$$\left. \begin{array}{l} (1) \text{ Eliminate } b^2: \\ a^2 - b^2 = 2a^2 - 1 = c \\ 2ab = s \end{array} \right\} \text{ Solve for } (a^2, ab) \rightarrow a^2 = \frac{1+c}{2}, \quad ab = \frac{s}{2} , \quad (11)$$

$$\text{Normalize or solve for } (a, b) \rightarrow a = \pm \frac{\sqrt{1+c}}{\sqrt{2}}, \quad b = \pm \frac{s}{\sqrt{2}\sqrt{1+c}} , \quad (12)$$

$$\left. \begin{array}{l} (2) \text{ Eliminate } a^2: \\ a^2 - b^2 = 1 - 2b^2 = c \\ 2ab = s \end{array} \right\} \text{ Solve for } (ab, b^2) \rightarrow ab = \frac{s}{2}, \quad b^2 = \frac{1-c}{2} , \quad (13)$$

$$\text{Normalize or solve for } (a, b) \rightarrow a = \pm \frac{s}{\sqrt{2}\sqrt{1-c}}, \quad b = \pm \frac{\sqrt{1-c}}{\sqrt{2}} . \quad (14)$$

The second set of solutions, Eqs. (12) and (14), is seen to be the same as the result of normalizing Eqs. (11) and (13), and these normalized forms are algebraically identical if we

multiply them by the ratios $\sqrt{1-c}/\sqrt{1-c}$ or $\sqrt{1+c}/\sqrt{1+c}$, respectively. *This clearly gives situations that require multiplying by 0/0*: the first normalized solution is impossible for $a \sim 0$, or $c \sim -1$, a perfectly legal rotation, and the second solution is impossible for $b \sim 0$, or $c \sim +1$, also perfectly legal! In addition, *both signs* in Eqs. (12) and (14) are valid, as we have the same rotation $R(a, b)$ if $(a, b) \rightarrow (-a, -b)$. The problem, actually an important *feature*, is that one normalized solution, Eq. (12), fails in one experimentally measurable domain, and the other, Eq. (14), fails in a *different* experimentally measurable domain. *Both must be considered together*, along with their opposite signs, in order to completely cover the full multivalued 720° range of θ parameterizing (a, b) . Those familiar with the long-standing quaternion extraction method of Shepperd (1978) may recognize some basic features appearing in a novel context here, and in the full quaternion treatment later on: there is in effect a condition on *which* rotation matrix elements can be trusted to produce a regular quaternion.

The left side of Fig. (2) shows how Eqs. (11) and (13) describe unit circles passing through the origin, with *distinct centers* at $(1, 0)$, $(0, 1)$, while their normalizations, Eqs. (12) and (14) for a and b , are unit *half circles* centered at $(0, 0)$, covering the positive x axis and the positive y axis, respectively. The two domains of the (a, b) solutions overlapping in the first quadrant work *together* to cover each other's singular normalization locations. This shows us unequivocally how the variables (a, b) and their multiple solutions describe a *manifold*, a topological space that cannot be described by a single function, but requires overlapping descriptions. Incorporating both signs of the circles of Eqs. (11) and (13), passing through the origin but with *distinct centers* at $(1, 0)$, $(0, 1)$, $(-1, 0)$, and $(0, -1)$, gives the completed picture illustrated in the right side of Fig. (2). The non-singular almost-half-circles (one sees a “half-pie” shape) resulting from normalization cover the entire range of four progressively overlapping domains that *together* describe the possible values of (a, b) over the whole range $0^\circ \leq \theta < 720^\circ$ with four local non-singular options.

Observe that, given the variables (a, b) , the four singularities in their solutions in terms of (c, s) occur when one variable or the other vanishes, $(a, b) \rightarrow (0, \pm 1)$ and $(a, b) \rightarrow (\pm 1, 0)$. We shall see in the full quaternion case that similar singularities occur in 14 submanifolds, the loci where any legal combination of quaternion elements vanishes, thus requiring similar multiple overlapping representations.

3.2 Variational Approach: the Bar-Itzhack Method in 2D

We now investigate the fact that the results of Section 3.1 can be seen in an alternative light by using a variational approach (Bar-Itzhack, 2000) rather than an algebraic approach. Seeing the quaternion appear as the solution to an eigensystem gives us a novel way, exploiting the adjugate formula introduced in Section 2, to see how singularities can be systematically resolved in this problem.

We begin by replacing the direct algebraic solution of the equations $R(c, s) = R(a, b)$

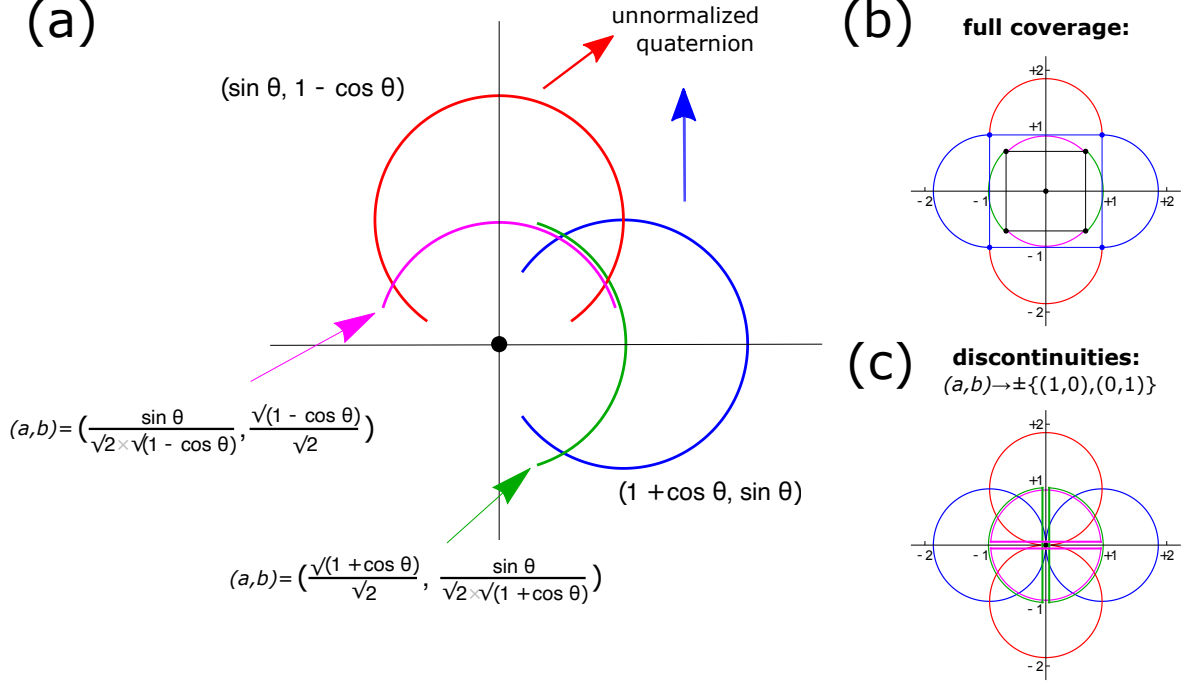


Figure 2: **Quaternion maps have discontinuities in 2D rotation space.** (a) The overlapping (a, b) regions in the positive quadrants. The normalized x axis region is in green, derived from the unnormalized region in blue, centered at $(1, 0)$; this sector is regular at 0° , and singular at $\pm 180^\circ$ (remember that for (a, b) , the range of θ is 720°). The normalized y axis region is in magenta, with corresponding singularities at 0° and 360° , derived from the unnormalized region in red, centered at $(0, 1)$, which is regular at 180° but singular at 0° and 360° . They overlap in the neighborhood of 90° , so, together, they are regular over an entire range in the parameters of (a, b) that covers 360° . (b) Each of the four unnormalized maps that cover the full quaternion space has a singularity in the normalization. The blue circles are the paths of $\pm(1 + c, s)$, mapping to the green half-circles in (a, b) , failing at $c = -1, a = 0$. The red circles are the paths of $\pm(s, 1 - c)$, mapping to the magenta half-circles in (a, b) , which fail at $c = +1, b = 0$. The curves along the positive axes, extending from -45° to 135° actually cover the whole rotation space; all four together span the entire quaternion space. (c) The discontinuities appear as singular limits when the outer circles close in on the origin, and the divide-by-zeros at those limits break the normalized circles half-way through, indicated by the four “half-pie” shapes, two in each color.

with what is essentially a least-squares formulation, minimizing the difference between the two matrices expressed using the Fröbenius norm,

$$\begin{aligned} L_{\text{Fröbenius}} &= \text{tr} \left((R(a, b) - R(c, s)) \cdot (R(a, b) - R(c, s))^t \right) \\ &= \text{tr} \left(I_2 + I_2 - 2R(a, b) \cdot R(c, s)^t \right) . \end{aligned} \quad (15)$$

At this point we can discard the constants and rephrase the problem of minimizing the least-squares version of the Fröbenius norm by a maximization of the cross-term, which we

choose to write as

$$\Delta_{\mathbf{F}} = \text{tr} \frac{1}{2} R(a, b) \cdot R(c, s)^{\text{t}} . \quad (16)$$

The task is now to maximize $\Delta_{\mathbf{F}}$ by finding $(a, b)_{\text{opt}}$ such that

$$(a, b)_{\text{opt}} = \underset{(a, b)}{\text{argmax}} \left(\text{tr} \frac{1}{2} R(a, b) \cdot R(c, s)^{\text{t}} \right) \quad (17)$$

– now regroup quadratic terms in (a, b) into left and right vectors:

$$= \underset{(a, b)}{\text{argmax}} \left([a, b] \cdot K(c, s) \cdot [a, b]^{\text{t}} \right) \equiv \underset{(a, b)}{\text{argmax}} \left([a, b] \cdot \begin{bmatrix} c & s \\ s & -c \end{bmatrix} \cdot [a, b]^{\text{t}} \right) . \quad (18)$$

We refer to the matrix $K(c, s)$, which has eigenvalues $\lambda = \pm 1$, as the *profile matrix* of the Bar-Itzhack optimization problem. From classical linear algebra (Golub and van Loan, 1983), we know that the task of maximizing $\Delta_{\mathbf{F}}$ is equivalent to identifying the maximal eigenvalue of the symmetric real matrix $K(c, s)$ and its eigenvector. The necessary eigenvalue is just $\lambda = +1$, and the corresponding eigenvector is just $(a, b)_{\text{opt}} = (\cos(\theta/2), \sin(\theta/2))$; this choice for (a, b) minimizes the Fröbenius norm Eq. (15), and in fact sets it to zero in this simplified example. But this misses the crucial information noted in Eqs. (12) and (14). A more formal and generalizable way to find the eigenvector, which can have any non-zero scale without changing the eigenvalue, is to form the characteristic equation's matrix, as noted in Section 2, by subtracting the eigenvalue $\lambda = +1$ from the diagonal,

$$\chi(c, s) = K(c, s) - (+1)I_2 = \begin{bmatrix} c-1 & s \\ s & -c-1 \end{bmatrix} , \quad (19)$$

and extract the eigenvector from $\chi(c, s)$. We now encounter the main point of this approach: the multiple forms of the solutions for (a, b) that we found by direct calculation earlier now appear *automatically* in the variational version. The crucial fact is that, given that the determinant of χ vanishes, $\det \chi \equiv 0$, *both adjugate columns* of the matrix χ are *unnormalized* eigenvectors of the given maximal eigenvalue.

For our case, we see that the two copies of the (unnormalized) maximal eigenvector are the two columns of the adjugate of χ :

$$\text{Adjugate}(\chi) = \left\{ \begin{bmatrix} -1-c \\ -s \end{bmatrix} , \begin{bmatrix} -s \\ -1+c \end{bmatrix} \right\} . \quad (20)$$

Since the eigenvectors are insensitive to overall sign and scale, we are free to multiply by $(-1/2)$ to get a more convenient form of the adjugate eigenvectors, which is

$$\text{AdjEigVectors}(\chi) = \left\{ \frac{1}{2} \begin{bmatrix} 1+c \\ s \end{bmatrix} , \frac{1}{2} \begin{bmatrix} s \\ 1-c \end{bmatrix} \right\} \quad (21)$$

We finally expose the *Adjugate Matrix* for our eigenvector representation by using the angle θ to rewrite Eq. (21) in terms of our 2D quaternion (a, b) ,

$$\text{Adjugate Matrix} = \begin{bmatrix} a^2 & ab \\ ab & b^2 \end{bmatrix}. \quad (22)$$

The problem here is by now familiar: neither eigenvector is a complete solution, as when we normalize, we find

$$\text{Normalized AdjEigVectors}(\chi) = \left\{ \begin{bmatrix} \frac{\sqrt{1+c}}{\sqrt{2}} \\ \frac{s}{\sqrt{2}\sqrt{1+c}} \end{bmatrix}, \begin{bmatrix} \frac{s}{\sqrt{2}\sqrt{1-c}} \\ \frac{\sqrt{1-c}}{\sqrt{2}} \end{bmatrix} \right\}. \quad (23)$$

The first column is singular at $c = -1$, the second column at $c = +1$, both completely legal points, but neither normalized adjugate column is a valid quaternion-like 2-vector for the *entire* range of the data (c, s) .

From Eq. (22), we can see clearly that both columns normalize to the eigenvector (a, b) since $a^2 + b^2 = 1$. But that eigenvector is multiplied by a in the first case, so no normalization is possible as $a \rightarrow 0$, and in the second column no normalization is possible as $b \rightarrow 0$. *Both pre-normalization columns* of the adjugate matrix must be included to cover the entire space of rotations; technically, due to the $(a, b) \rightarrow (-a, -b)$ equivalence, the full topological space of (a, b) of course actually has four natural components. (See Figure 2.) To reiterate, the reason for this is that only a^2 , b^2 , and ab , the quadratic forms, can actually be expressed in terms of the measurable rotation matrix data (c, s) . We must have access to the *entire* adjugate matrix because the entire circular quaternion path of (a, b) describes a multivalued *manifold*, not a single-valued *function*. With the conventional configuration of neural nets that only approximate functions, one can never determine a global solution for (a, b) directly, but must target the multiple-valued *adjugate matrix* of locally normalizable solutions, with the choice of adjugate column occurring as a final data-driven post-processing step. It is worthwhile noting that this is essentially the same type of process involved in the classic multiple-choice Shepperd algorithm (Shepperd, 1978) for extracting a quaternion from a 3D rotation matrix, but with the clearer purely linear algebraic adjugate-matrix context that arises naturally in the Bar-Itzhack variational approach.

3.3 Bar-Itzhack Errorful Measurement Strategy in 2D

We have thus far assumed that measurements of a rotation matrix resulted in a perfect orthonormal matrix. That strategy allowed us to clearly expose the requirement to use a multivalued formula to find the 2D quaternion analog (a, b) from the parameters (c, s) of an ideal orthonormal measured rotation matrix. The same basic approach is valid also for

inaccurate measurements that report rotation matrix elements that are not orthonormal. The basic ideas appear in the original work of (Shepperd, 1978) and of Bar-Itzhack (2000), while further details of the 2D case appear in Haralick et al. (1989) and in the Supplementary Material of Hanson (2020).

To see how to work with inaccurate rotation matrix measurements, we introduce the “measured matrix data” $R(m)$,

$$R(m) = \begin{bmatrix} m_{11} & m_{12} \\ m_{21} & m_{22} \end{bmatrix}. \quad (24)$$

Comparing this to our ideal quadratic quaternion-like target for the same matrix, Eq. (9), we immediately encounter the problem that we have two variables in $R(a, b)$ and four variables in $R(m)$. We cannot solve directly for the 2D (a, b) quadratic forms, and, unsurprisingly, this problem still arises in 3D, as we will see below.

We now argue that for noisy data, we gain clarity by applying the Bar-Itzhack optimization approach, and that its validity is much easier to understand and justify. We begin with Eq. (24) and insert it into the Fröbenius norm for the distance between $R(m)$ and Eq. (9) for $R(a, b)$, yielding

$$\begin{aligned} S_{\mathbf{F}} &= \text{tr} (R(a, b) - R(m)) \cdot (R(a, b) - R(m))^{\text{t}} \\ &= (a^2 - b^2 - m_{11})^2 + (2ab + m_{12})^2 + (2ab - m_{21})^2 + (a^2 - b^2 - m_{22})^2 \\ &= 2 + \sum_{i,j} (m_{ij})^2 - 2(a^2 - b^2)(m_{11} + m_{22}) + 4ab(m_{12} - m_{21}). \end{aligned} \quad (25)$$

We strip the constants and change the sign to turn the problem of minimizing $S_{\mathbf{F}}$ to the equivalent problem of maximizing the cross term, which, as before, we can now write immediately as this matrix product defining the profile matrix $K(m)$:

$$\begin{aligned} \Delta_{\mathbf{F}} &= (a^2 - b^2)(m_{11} + m_{22}) + 2ab(m_{21} - m_{12}) \\ &= [a \ b] \cdot \begin{bmatrix} (m_{11} + m_{22}) & (m_{21} - m_{12}) \\ (m_{21} - m_{12}) & -(m_{11} + m_{22}) \end{bmatrix} \cdot [a \ b]^{\text{t}} \equiv [a \ b] \cdot K(m_{ij}) \cdot [a \ b]^{\text{t}}. \end{aligned}$$

The solution to our optimization problem

$$[a \ b]_{\text{opt}} = \underset{(a, b)}{\text{argmax}} [a \ b] \cdot K(m) \cdot [a \ b]^{\text{t}} \quad (26)$$

is then reduced to finding the eigenvector $[a, b]_{\text{opt}}$ corresponding to the maximal eigenvalue of $K(m)$. Since $\text{tr}[K(m)] = 0$, the eigenvalues are an opposite-sign pair, with the maximal eigenvalue being the positive choice

$$\lambda_{\text{max}} = \sqrt{(m_{11} + m_{22})^2 + (m_{12} - m_{21})^2} \quad (27)$$

Note that the appearance of only the antisymmetric part of the off-diagonal terms in $R(m)$ is an inevitable consequence of the optimization of the Fröbenius norm Eq. (25).

The final step is to cover the entire manifold of solutions for the multivalued (a, b) using the adjugate matrix of the maximal eigensystem,

$$\begin{aligned} \text{Adj}([K(m) - \lambda_{\max} I_2]) &= \\ &= \left\{ \begin{bmatrix} -(m_{11} + m_{22}) - \lambda_{\max} & \\ & m_{12} - m_{21} \end{bmatrix}, \begin{bmatrix} & m_{12} - m_{21} \\ (m_{11} + m_{22}) - \lambda_{\max} & \end{bmatrix} \right\} \end{aligned} \quad (28)$$

We see immediately the automatic appearance of a pair of solutions for $[a, b]_{\text{opt}}$ that have singularities in different places when normalized, thus covering, with their negative counterparts, the entire manifold of (a, b) . Since the eigenvectors represented by the columns of the adjugate matrix are insensitive to rescaling, we can transform Eq. (28) to a more readable form by changing the sign and denoting the trace and antisymmetric off-diagonal terms as follows:

$$d = \frac{1}{2} (m_{11} + m_{22}) \quad t = \frac{1}{2} (m_{21} - m_{12}) \quad \lambda = \sqrt{d^2 + t^2}. \quad (29)$$

We note that if our matrix were to be a pure rotation, we would have $d = \cos \theta$ and $t = \sin \theta$, so $\lambda = 1$. We find the unnormalized eigenvector pairs

$$\text{Adjugate eigenvectors} = \left\{ \pm \begin{bmatrix} \sqrt{t^2 + d^2} + d \\ t \end{bmatrix}, \pm \begin{bmatrix} t \\ \sqrt{t^2 + d^2} - d \end{bmatrix} \right\} \quad (30)$$

$$= \left\{ \pm \begin{bmatrix} \lambda + d \\ t \end{bmatrix}, \pm \begin{bmatrix} t \\ \lambda - d \end{bmatrix} \right\}. \quad (31)$$

Equation (31) is the exact analog for errorful rotations of the adjugate matrix Eq. (22). Normalizing Eq. (31) to obtain quaternions, we see as before that the two versions are equivalent except at singular points, but that one is always a computable normalized eigenvector:

$$\text{normalized Adj eigenvectors} = \left\{ \pm \begin{bmatrix} \frac{\sqrt{\lambda + d}}{\sqrt{2}\sqrt{\lambda}} \\ \frac{t}{\sqrt{2}\sqrt{\lambda(\lambda + d)}} \end{bmatrix}, \pm \begin{bmatrix} \frac{t}{\sqrt{2}\sqrt{\lambda(\lambda - d)}} \\ \frac{\sqrt{\lambda - d}}{\sqrt{2}\sqrt{\lambda}} \end{bmatrix} \right\}. \quad (32)$$

Observe that the numerical eigenvalue λ appears throughout in just such a way that if we have $\lambda = 1$, we have precisely the previous solution Eq. (23) for the normalized set of maximal eigenvectors. It is worth noting that while Eq. (29) was mentioned in the supplement to (Hanson, 2020), the importance of the adjugate and the singularities in the rotation-to-quaternion mappings of Eqs. (31) and (32) were yet to be recognized.

3.4 Summary

In this section, we have worked through the simple case of two dimensional rotations by an angle θ , in parallel with how that corresponds to the 2D simplification of the quaternion-parameterized rotation matrix in Eq. (1) to a 2D version written in terms of the reduced quaternion (a, b) . This has led us to the understanding that in order to solve for (a, b) in terms of the elements of a 2D measured rotation matrix, we must have two separate sectors, one regular at $(1, 0)$ and singular at $(0, 1)$, and the other reversed. To account for the full quaternion space where both (a, b) and $(-a, -b)$ correspond to the same 2D rotation $R(a, b)$, we in fact need four sectors covering the full circular manifold of the quaternion space. We have also seen that the techniques that reveal the manifold properties of the quaternion space also give us a way to find the *optimal* exact rotation corresponding to a noisy set of rotation matrix data. In the next Section, we perform a parallel analysis for 3D rotations and full quaternions, deriving and studying the results previewed in Section 2. We will again find that the clearest understanding of this problem is based on the adjugate matrix arising in the Bar-Itzhack optimization algorithm, and that noisy input data in particular are most clearly treated in this way.

4 Three-Dimensional Rotations and the Quaternion Map

We now turn to the realistic case of interest, how to correctly determine a quaternion corresponding to a measured 3D rotation matrix, and presenting a complete derivation and explanation of the results summarized in Section 2. As in Section 3, we will begin with a direct derivation using only the symbolic forms of the quaternion-rotation problem, followed by the Bar-Itzhack variational version of the same problem, which will exhibit some new features. Again, the multivalued target required for, e.g., a rigorous formulation of a machine learning process, will be expressed in terms of an adjugate matrix. We conclude with the corresponding variational treatment of noisy inexact rotation measurements producing the optimal true rotation matrix deduced from the noisy measured approximate rotation matrix data.

4.1 Direct Solution of the Three-Dimensional Problem

A *proper* orthonormal 3D rotation matrix can be written as a quadratic form $R(q)$ in the quaternion elements $q = (q_0, q_1, q_2, q_3)$, with $q \cdot q = 1$, and identified with the axis-angle form $R(\theta, \hat{\mathbf{n}})$ as follows

$$R(q) = R(\theta, \hat{\mathbf{n}}) \tag{33}$$

$$\begin{aligned}
& \begin{bmatrix} q_0^2 + q_1^2 - q_2^2 - q_3^2 & 2q_1q_2 - 2q_0q_3 & 2q_1q_3 + 2q_0q_2 \\ 2q_1q_2 + 2q_0q_3 & q_0^2 - q_1^2 + q_2^2 - q_3^2 & 2q_2q_3 - 2q_0q_1 \\ 2q_1q_3 - 2q_0q_2 & 2q_2q_3 + 2q_0q_1 & q_0^2 - q_1^2 - q_2^2 + q_3^2 \end{bmatrix} \\
&= \begin{bmatrix} c + (1-c)\hat{n}_1^2 & (1-c)\hat{n}_1\hat{n}_2 - s\hat{n}_3 & (1-c)\hat{n}_1\hat{n}_3 + s\hat{n}_2 \\ (1-c)\hat{n}_1\hat{n}_2 + s\hat{n}_3 & c + (1-c)\hat{n}_2^2 & (1-c)\hat{n}_2\hat{n}_3 - s\hat{n}_1 \\ (1-c)\hat{n}_1\hat{n}_3 - s\hat{n}_2 & (1-c)\hat{n}_2\hat{n}_3 + s\hat{n}_1 & c + (1-c)\hat{n}_3^2 \end{bmatrix}, \quad (34)
\end{aligned}$$

where $\hat{\mathbf{n}} \cdot \hat{\mathbf{n}} = 1$ and we abbreviate $c = \cos \theta$, $s = \sin \theta$. As noted earlier, $\hat{\mathbf{n}}$ is the fixed axis about which we rotate by the angle θ , and parameterizing the quaternion as

$$q(\theta, \hat{\mathbf{n}}) = (\cos(\theta/2), \hat{n}_1 \sin(\theta/2), \hat{n}_2 \sin(\theta/2), \hat{n}_3 \sin(\theta/2)) \quad (35)$$

exactly reproduces $R(\theta, \hat{\mathbf{n}})$. We can easily rearrange Eq. (34) (or just apply $q(\theta, \hat{\mathbf{n}})$) to produce an explicit solution for the 10 quadratic forms in q , written in terms a 4×4 symmetric matrix that will turn out to be important in our narrative:

$$\begin{bmatrix} q_0^2 & q_0q_1 & q_0q_2 & q_0q_3 \\ q_0q_1 & q_1^2 & q_1q_2 & q_1q_3 \\ q_0q_2 & q_1q_2 & q_2^2 & q_2q_3 \\ q_0q_3 & q_1q_3 & q_2q_3 & q_3^2 \end{bmatrix} = \frac{1}{2} \begin{bmatrix} 1+c & sn_1 & sn_2 & sn_3 \\ sn_1 & (1-c)n_1^2 & (1-c)n_1n_2 & (1-c)n_1n_3 \\ sn_2 & (1-c)n_1n_2 & (1-c)n_2^2 & (1-c)n_2n_3 \\ sn_3 & (1-c)n_1n_3 & (1-c)n_2n_3 & (1-c)n_3^2 \end{bmatrix}. \quad (36)$$

Equation (36) is the full quaternion analog of the unnormalized 2D Equations (11) and (13), where we note that $(c, s) = (\cos \theta, \sin \theta)$ are in terms of the full angle, not the half-angle quaternion form. In Eqs. (12) and (14), we wrote out the explicit normalized quaternions and noted the two distinct singularities at $c = +1$, $c = -1$. Here we choose to analyze the normalization factors separately to clarify the analysis. Obviously each row of Eq. (36) is normalized to a *symbolically correct* quaternion $q = (q_0, q_1, q_2, q_3)$ by normalizing, in row-wise sequence, by

$$\begin{aligned}
\text{row 0: } \frac{1}{q_0} &= \frac{1}{\cos(\theta/2)} = \sqrt{\frac{2}{1+c}} \\
\text{row 1: } \frac{1}{q_1} &= \frac{1}{n_1 \sin(\theta/2)} = \frac{1}{n_1} \sqrt{\frac{2}{1-c}} \\
\text{row 2: } \frac{1}{q_2} &= \frac{1}{n_2 \sin(\theta/2)} = \frac{1}{n_2} \sqrt{\frac{2}{1-c}} \\
\text{row 3: } \frac{1}{q_3} &= \frac{1}{n_3 \sin(\theta/2)} = \frac{1}{n_3} \sqrt{\frac{2}{1-c}}.
\end{aligned} \quad (37)$$

We observe that there are singularities in the normalization factors at new locations *in addition* to the $c = \pm 1$ singularities appearing in the 2D case. This is easy to understand: our expression for $q(\theta, \hat{\mathbf{n}})$ is arbitrary, and any permutation of the parameter elements is equally valid, so the singularities *should* be spread among the components without singling out any

given one. We can conclude that the 4D analog of the 2D pair of $(a, b) \rightarrow \pm\{(1, 0), (0, 1)\}$ singularities in the normalization is in fact this set of 14 distinct cases:

$$\begin{aligned}
\text{one zero} &\rightarrow \{(0, x, y, z), (x, 0, y, z), (x, y, 0, z), (x, y, z, 0)\} \\
\text{two zeroes} &\rightarrow \{(0, 0, x, y), (0, x, 0, y), (0, x, y, 0), (x, 0, 0, y), (x, 0, y, 0), (x, y, 0, 0)\} \quad , \\
\text{three zeroes} &\rightarrow \pm\{(1, 0, 0, 0), (0, 1, 0, 0), (0, 0, 1, 0), (0, 0, 0, 1)\}
\end{aligned} \tag{38}$$

where $x^2 + y^2 + z^2 = 1$ in the first line and $x^2 + y^2 = 1$ in the second line to preserve $q \cdot q = 1$. Since the first two cases are spheres \mathbf{S}^2 and \mathbf{S}^1 , the sign option \pm in the third case is included; in fact, a more general way to think of the points ± 1 is as just another sphere, the zero-sphere \mathbf{S}^0 solving $x^2 = 1$. The key of course is that, since $q \cdot q = 1$, there always has to be at least one element with $|q_i| \geq 1/2$, and thus we can always find a row that is normalizable. These fourteen unnormalizable regions of the quaternion solution for a given rotation are illustrated in Figure 3. In Appendix D, Eq. (121), we list the explicit adjugate matrices observed when each of these anomalies occurs, along with visualizations in Figures (8) and (9).

A standard choice for selecting a well-defined solution from the 4×4 matrix of alternate quaternion solutions, in parallel to the algorithm of Shepperd (1978), is to note that the diagonal of the left-hand side of Eq. (36) is simply $\{q_0^2, q_1^2, q_2^2, q_3^2\}$, so if we identify the ordinal location k of the maximal diagonal q_k^2 , that is the row we normalize:

$$\textbf{Normalizable solution: } q_{\text{opt}} = \frac{\pm 1}{|q_k|} (q_0 q_k, q_1 q_k, q_2 q_k, q_3 q_k) \quad . \tag{39}$$

The sign is of course arbitrary, though a standard choice is to make $q_0 > 0$ when possible. The significance of this for our problem is that, because the quaternion sphere \mathbf{S}^3 is a topological manifold that cannot be described by a single function produced by a neural net, any algorithm that needs to find *a universally applicable quaternion* must produce a *list of four candidates corresponding to the columns of Eq. (36)*, remembering that there are 14 ways to fail normalizing any single one, and choose a normalizable candidate from that list to produce a usable quaternion via Eq. (39).

4.2 Variational Approach: Bar-Itzhack in 3D

The variational method we presented for finding $(a, b)_{\text{opt}}$ from experimental 2D rotation matrix data extends straightforwardly to the 3D case to determine q_{opt} . The basic ideas appear in Bar-Itzhack (2000), with some refinements in Appendix C and the Supplementary Material of Hanson (2020); see also Sarabandi et al. (2018, 2020).

The full 3D problem consists of finding the 4D quaternion $q_{\text{opt}} = (q_0, q_1, q_2, q_3)$ such that $R(q_{\text{opt}})$ best describes a measured 3D numerical rotation matrix R . We begin as before

with the ideal symbolic case, which is now $R = R(\theta, \hat{\mathbf{n}})$. The task is to exploit quaternion features to minimize the Fröbenius norm of the difference between the two matrices, where our initial optimization measure is

$$\begin{aligned} \mathbf{L}_{\text{Fröbenius}} &= \text{tr} \left((R(q) - R(\theta, \hat{\mathbf{n}})) \cdot (R(q) - R(\theta, \hat{\mathbf{n}}))^{\text{t}} \right) \\ &= \text{tr} \left(I_3 + I_3 - 2R(q) \cdot R(\theta, \hat{\mathbf{n}})^{\text{t}} \right) . \end{aligned} \quad (40)$$

At this point we can discard the constants and rephrase the problem of minimizing the least-squares version of the Fröbenius norm in terms of maximizing the cross-term, which we choose to write as

$$\Delta_{\mathbf{F}} = \text{tr} R(q) \cdot R(\theta, \hat{\mathbf{n}})^{\text{t}} = q \cdot K(\theta, \hat{\mathbf{n}}) \cdot q . \quad (41)$$

where expanding $R(q)$ using the form of Eq. (34) allows us to rewrite the trace in Eq. (41) as matrix product using the *profile matrix*

$$K_0(\theta, \hat{\mathbf{n}}) = \begin{bmatrix} 2c + 1 & 2s \hat{n}_1 & 2s \hat{n}_2 & 2s \hat{n}_3 \\ 2s \hat{n}_1 & 2(1 - c) \hat{n}_1^2 - 1 & 2(1 - c) \hat{n}_1 \hat{n}_2 & 2(1 - c) \hat{n}_1 \hat{n}_3 \\ 2s \hat{n}_2 & 2(1 - c) \hat{n}_1 \hat{n}_2 & 2(1 - c) \hat{n}_2^2 - 1 & 2(1 - c) \hat{n}_2 \hat{n}_3 \\ 2s \hat{n}_3 & 2(1 - c) \hat{n}_1 \hat{n}_3 & 2(1 - c) \hat{n}_2 \hat{n}_3 & 2(1 - c) \hat{n}_3^2 - 1 \end{bmatrix} . \quad (42)$$

The task is now to maximize $\Delta_{\mathbf{F}}$ by finding q_{opt} such that

$$q_{\text{opt}} = \underset{q}{\text{argmax}} \left(\text{tr} R(q) \cdot R(\theta, \hat{\mathbf{n}})^{\text{t}} \right) = \underset{q}{\text{argmax}} (q \cdot K(\theta, \hat{\mathbf{n}}) \cdot q) . \quad (43)$$

Since $K_0(\theta, \hat{\mathbf{n}})$ is a symmetric real matrix, the maximum of $q \cdot K_0 \cdot q$ is achieved by picking out the maximal eigenvalue, so the corresponding q_{opt} is the maximal eigenvector. The eigenvalues of $K_0(\theta, \hat{\mathbf{n}})$ are $\lambda = (3, -1, -1, -1)$, so all we need to do is find the eigenvector of $\lambda = 3$. However, we will first use some linear algebra manipulations to simplify the appearance of our equations. We note that

- Since the characteristic equation we used to solve for the eigenvalues is $\det(K_0 - \lambda I_4) = 0$, *adding a constant* to K_0 simply adds the same constant to the eigenvalues, while *scaling* K_0 simply scales the eigenvalues by a constant.
- The eigenvectors of any well-behaved eigensystem can be computed from the *adjugate matrix* of the vanishing-determinant characteristic equation into which a valid eigenvalue has been substituted. This follows from the fact that for any matrix, $M \cdot \text{Adj}(M) = \det M I_4$; the latter equation also indicates that the four columns of $\text{Adj}(K_0)$ are all formally eigenvectors of the *same eigenvalue*.
- The eigenvectors themselves can be multiplied by any non-vanishing scale factor without changing the eigenvalue equation, since the eigenvector equation is homogenous in the eigenvector itself.

Therefore, we can replace our original matrix $K_0(\theta, \hat{\mathbf{n}})$ in Eq. (42) by adding one copy of the identity matrix and dividing by 4 to yield a new matrix

$$K(\theta, \hat{\mathbf{n}}) = \frac{1}{4} (K_0(\theta, \hat{\mathbf{n}}) + 1 \times I_4) = \frac{1}{2} \begin{bmatrix} 1+c & s\hat{n}_1 & s\hat{n}_2 & s\hat{n}_3 \\ s\hat{n}_1 & (1-c)\hat{n}_1^2 & (1-c)\hat{n}_1\hat{n}_2 & (1-c)\hat{n}_1\hat{n}_3 \\ s\hat{n}_2 & (1-c)\hat{n}_1\hat{n}_2 & (1-c)\hat{n}_2^2 & (1-c)\hat{n}_2\hat{n}_3 \\ s\hat{n}_3 & (1-c)\hat{n}_1\hat{n}_3 & (1-c)\hat{n}_2\hat{n}_3 & (1-c)\hat{n}_3^2 \end{bmatrix}. \quad (44)$$

whose eigenvalues are now $(1, 0, 0, 0)$, so the maximal eigenvalue is now $\lambda_{\text{opt}} = 1$, but whose normalized eigenvectors are preserved. $K(\theta, \hat{\mathbf{n}})$ has some interesting properties. First, we see from Eq. (35) for $q(\theta, \hat{\mathbf{n}})$ that we have simply rediscovered Eq. (36), except that now we perceive it in a new light, as the root of an eigensystem whose maximal eigenvector determines q_{opt} . Furthermore, whichever of the two forms of $K(\theta, \hat{\mathbf{n}}) = K(q)$ we use, the eigenvectors corresponding to the eigenvalues are just

$$\left\{ \begin{bmatrix} q_0 \\ q_1 \\ q_2 \\ q_3 \end{bmatrix}, \begin{bmatrix} -q_1 \\ q_0 \\ 0 \\ 0 \end{bmatrix}, \begin{bmatrix} -q_2 \\ 0 \\ q_0 \\ 0 \end{bmatrix}, \begin{bmatrix} -q_3 \\ 0 \\ 0 \\ q_0 \end{bmatrix} \right\}. \quad (45)$$

and the quaternion itself, $q = (q_0, q_1, q_2, q_3)$ is trivially the maximal eigenvector with $\lambda_{\text{opt}} = 1$.

However, there is a deeper meaning in the eigensystem generated by the Bar-Itzhack variational method that tells us everything that is important about the non-trivial manifold in which quaternions live. *Given the profile matrix K* , we can compute the maximal eigenvector corresponding to $\lambda_{\text{opt}} = 1$ simultaneously in four different ways by writing down the characteristic equation of K with $\lambda = 1$ and computing the 4×4 *adjugate matrix*. We can use any equivalent form we like, but $K(q)$ is particularly simple: first we examine

$$\text{characteristic equation: } = \chi = K(q) - 1 \times I_4 \quad (46)$$

$$= K(q) - (q \cdot q) \times I_4, \quad (47)$$

and then remarkably, when we compute the adjugate of the maximal eigenvalue's characteristic equation for $K(q)$, we find it is simply *the negative of $K(q)$ itself*:

$$\text{Adjugate}(\chi) = - \begin{bmatrix} q_0^2 & q_0q_1 & q_0q_2 & q_0q_3 \\ q_0q_1 & q_1^2 & q_1q_2 & q_1q_3 \\ q_0q_2 & q_1q_2 & q_2^2 & q_2q_3 \\ q_0q_3 & q_1q_3 & q_2q_3 & q_3^2 \end{bmatrix} = -K(q). \quad (48)$$

Recall that the minus sign can be removed and the positive quadratic matrix employed to represent the family of alternative unnormalized maximal eigenvectors, since the eigenequation is insensitive to the scale of the eigenvectors. We already know these solutions for

q_{opt} are correct, since each row (or column, as it is symmetric) is proportional to the maximal eigenvector $q = (q_0, q_1, q_2, q_3)$. However, in addition we observe a repetition of our observation in Section 4.1 that the four rows of superficially equivalent solutions are *not* equivalent, but indicate that any of the fourteen combinations of appearances of zeroes in one, two, or three of the quaternion components (q_0, q_1, q_2, q_3) renders the entire row useless for computing the correct quaternion corresponding to the measured rotation matrix, and another quadratic row with nonsingular normalization must be used for the calculation.

4.3 Bar-Itzhack Variational Approach to 3D Noisy Data

We have found the solution for the quaternion manifold's four solutions (eight with signs) in terms of a perfect orthogonal measurement of the rotation data. As noted by Bar-Itzhack (2000), the same basic procedure can be used for measured rotation matrices with errors, and the resulting quaternion produces a perfect orthonormal rotation matrix that is the *optimal approximation* to the provided errorful data. The issue of handling rotation data with wide-ranging errors has been studied by Sarabandi et al. (2018); their heuristic approach to determining an optimal rotation omits critical steps in the noisy-data treatment of Bar-Itzhack that we handle rigorously here. Our starting point is a measured 3×3 matrix $R(m)$ that is assumed to originate from a 3D rotation matrix, but cannot be guaranteed to be orthonormal due to measurement error; we write the components of this input data matrix as

$$R(m) = \begin{bmatrix} m_{11} & m_{12} & m_{13} \\ m_{21} & m_{22} & m_{23} \\ m_{31} & m_{32} & m_{33} \end{bmatrix}. \quad (49)$$

We set up the Bar-Itzhack variational problem starting with a symbolic rotation in the quadratic quaternion form $R(q)$ given in Eq. (1), and write down the cross-term of the Fröbenius norm to define a maximization problem that will be our optimization target:

$$\Delta_{\mathbf{F}}(q, m) = \text{tr } R(q) \cdot R(m)^{\text{t}} = q \cdot K_0(m) \cdot q. \quad (50)$$

Our initial profile matrix resulting from rearranging the quadratic quaternion terms into the form of a scalar-valued symmetric matrix multiplication takes the form

$$K_0(m) = \begin{bmatrix} m_{11} + m_{22} + m_{33} & m_{32} - m_{23} & m_{13} - m_{31} & m_{21} - m_{12} \\ m_{32} - m_{23} & m_{11} - m_{22} - m_{33} & m_{12} + m_{21} & m_{13} + m_{31} \\ m_{13} - m_{31} & m_{12} + m_{21} & -m_{11} + m_{22} - m_{33} & m_{23} + m_{32} \\ m_{21} - m_{12} & m_{13} + m_{31} & m_{23} + m_{32} & -m_{11} - m_{22} + m_{33} \end{bmatrix} \quad (51)$$

Note that $K_0(m)$ is traceless, and since $K_0(m)$ is a real symmetric matrix, it will have real eigenvalues. The eigenvector q_{opt} of $K_0(m)$'s maximal eigenvalue $\lambda_{\text{opt}}(m)$ will maximize

$\Delta_{\mathbf{F}}(q, m)$. This maximal eigensystem will solve the optimization problem

$$q_{\text{opt}} = \underset{q}{\operatorname{argmax}} \left(\operatorname{tr} R(q) \cdot R(m)^{\dagger} \right) = \underset{q}{\operatorname{argmax}} (q \cdot K_0(m) \cdot q) \quad (52)$$

$$\lambda_{\text{opt}} = \Delta_{\mathbf{F}}(q_{\text{opt}}, m) = (q_{\text{opt}} \cdot K_0(m) \cdot q_{\text{opt}}) \quad (53)$$

However, to be a proper quaternion, the optimizing value of the eigenvector q of λ_{opt} will have to be normalized to become q_{opt} , and we have argued throughout that this is not always possible, and must be dealt with using the quaternionic manifold \mathbf{S}^3 with eight covering coordinate patches instead of relying on a single function.

Fortunately, we know from the exact-rotation-data case in the preceding section how to deal correctly with this issue in the Bar-Itzhack context. We note that while it was useful in the exact case to get a very clean set of formulas by performing an eigenvector-preserving transformation of the form

$$K(m) = \text{scale} \times (K_0(m) + \text{constant} \times I_4) \quad (54)$$

to adjust our maximal eigenvalue to the identity, in the general case, we cannot find a single pair of constants that will be all that useful, though one might choose to normalize to obtain a unit maximal eigenvalue by dividing by the value of K_0 's maximal eigenvalue $\lambda_{\text{opt}}(m)$. We will assume that if there is some reason to readjust $K_0(m)$ to a form $K(m)$ with the same eigenvectors, up to scaling, preserving the corresponding maximal eigenvalue $\lambda_{\text{opt}}(m)$ up to an additive constant, we may do so, and thus we will continue with that abstract $K(m)$ to complete our argument.

Obviously what we have to do first is find $\lambda_{\text{opt}}(m)$. Standard numerical eigensystem software packages can easily accomplish this, and, for symmetric real matrices up to 4×4 in size, one can even calculate the maximal eigenvalue analytically using Cardano's solution of 4th degree polynomials (see, e.g, Hanson (2020) for a review). The last step is then to form the characteristic equation's matrix as before, using now the *numerical* eigenvalue, giving

$$\begin{aligned} \text{characteristic matrix: } &= \chi(m) = K(m) - \lambda_{\text{opt}}(m) \times I_4 \\ &= K(m) - (q_{\text{opt}} \cdot K(m) \cdot q_{\text{opt}}) \times I_4 \end{aligned} \quad (55)$$

where

$$\det \chi(m) \equiv 0 \quad .$$

Finally, our full quaternion-space covering manifold solution is determined from the adjugate of Eq. (55), which is an entirely numerical matrix having the following (possibly scaled) relation to the sign-ambiguous set of eight possible quaternion formulas:

$$\begin{bmatrix} q_0^2 & q_0 q_1 & q_0 q_2 & q_0 q_3 \\ q_0 q_1 & q_1^2 & q_1 q_2 & q_1 q_3 \\ q_0 q_2 & q_1 q_2 & q_2^2 & q_2 q_3 \\ q_0 q_3 & q_1 q_3 & q_2 q_3 & q_3^2 \end{bmatrix} = \text{Adjugate}(\chi(m)) \quad (56)$$

Recall that the adjugate is determined only up to a nonvanishing scale of either sign, and that one picks the ordinal index k with the largest diagonal value q_k^2 in the adjugate matrix, and normalizes that row to obtain q_{opt} . Finally, one calculates the *optimal pure rotation approximation* to the numerically measured $R(m)$ using this quaternion selected from the adjugate matrix:

$$R_{\text{opt}}(m) = R(q_{\text{opt}}) \quad (57)$$

and our treatment of how to compute a quaternion from any ideal or noisy rotation matrix data is done.

4.4 Graphical Illustration of the 3D Rotation Case

We can get an intuitive feeling for what is going on with the multiple valid regions for the quaternion solution representations by drawing representative spaces corresponding to the unnormalized (and potentially singular) solutions, and then making pointwise normalization maps from those spaces to the actual quaternion subspaces, and noting where validity of the normalization map fails.

In 2D, these maps were fairly simple to see in Figure 2, where a simple unnormalized circle mapped to a half-circle in the 2D reduced quaternion plane. Going one step higher in complexity, we can produce images in 2D that correspond to a quaternion map, but one dimension lower. The top part of Figure 3 illustrates pairs of 2D spheres embedded in \mathbb{R}^3 centered at $(\pm 1, 0, 0)$, $(0, \pm 1, 0)$, and $(0, 0, \pm 1)$, shown in red. Taking each point on the red spheres and applying the normalization operation, we obtain the green spheres centered at the origin $(0, 0, 0)$. As the red spheres' points approach the origin, the normalization approaches a divide-by-zero at the equator of each green sphere, and the map can go no farther.

The bottom part of Figure 3 illustrates the geometry in quaternion space of the 14 singular subspaces, where one or more normalizations of quaternion parameterizations in terms of rotation matrices will fail, and a test must be made to identify a legal normalization step. When one of the four sets of three vanishing quaternions occurs, only the point pair at the tip of a 4D axis is permitted, as shown in the left bottom part of the figure. If one of six pairs of zeros occurs, the six circles in the middle part denote the allowed subspace of quaternions, and if only one quaternion vanishes, there are four allowed spherical subspaces as shown at the left. These fourteen collections of 4, 6, and 4 subspaces correspond roughly to the vertices, edges, and faces of a complex tetrahedron, as a tetrahedron has 4 vertices, 6 edges, and 4 faces. Additional illustrations of the higher dimensional properties of these singularities are given in Appendix D, Figures (8) and (9).

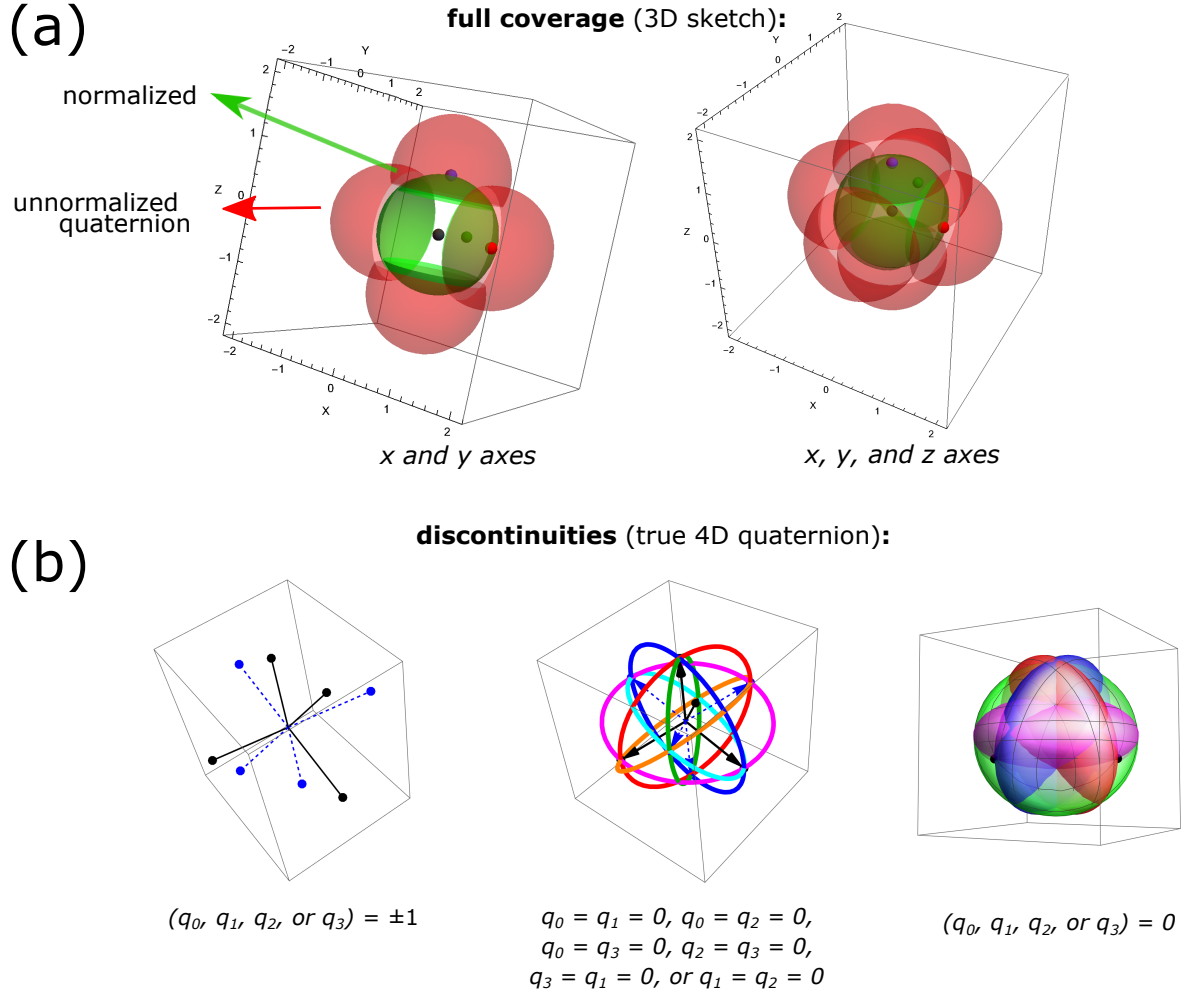


Figure 3: (a) **3D subspace showing three axes of singularities.** In this 3D subspace of quaternion space, there are partial spheres instead of partial circles as in 2D, but the singularity occurs in the same way: as the sphere closes in on the origin, normalization is impossible. At left, the x and y axes coincide with the four red spheres that produce partial coverings for the inner green quaternion-subspace spheres. At the right, we include the z axis component and show all six singularity-limited quaternion-subspace normalized hemispheres in green, giving the 3D analog of the 2D case Fig. (2).

(b) **Visualizing the fourteen quaternion singular-normalization domains.** (Left) The allowed quaternions if any three components vanish are the four \mathbf{S}^0 subspaces at the ends of the 4D axes, $q_0 = \pm 1$, $q_1 = \pm 1$, $q_2 = \pm 1$, and $q_3 = \pm 1$. (Middle) Allowed quaternions with two zeroes are six topological circles \mathbf{S}^1 . A single circle projected to 3D from the unit quaternion with $q_0 = q_1 = 0$ is just the curve $(0, 0, x, y)$ with $x^2 + y^2 = 1$. The union of all six curves matches the six edges of a complex tetrahedron. (Right) Regions of singularity for quaternions with a single zero are topological spheres \mathbf{S}^2 that correspond to four faces of a complex tetrahedron, with the allowed $q_0 = 0$ subspace, for example, being the spherical surface $(0, x, y, z)$ with $x^2 + y^2 + z^2 = 1$.

5 Applications of the Adjugate Representation

We now apply the quaternion adjugate variable representation to the classic problems of estimating the optimal rotations needed to align sets of pointwise matched data. The basic appearance of the data for each of the problems we shall treat is summarized visually in Fig. (1) in the Introduction. We first examine in sections 5.1 and 5.2 the simple but pedagogically instructive 2D cloud problems, namely matching rotation-related pairs of 2D clouds, and then pose discovery given a 2D cloud and a 1D point-matched image derived from that cloud. The more relevant 3D cloud matching case has been solved in many ways, so again our adjugate variable approach in section 5.3 is mainly of pedagogical interest. The reader will find the most interesting results in section 5.4, in which we exploit the adjugate reduction in the power of the least squares loss function for orthographic 3D-cloud-to-2D-image matching, discovering a new closed form solution to that least squares problem. Finally, in section 5.5, we apply the methods of our orthographic pose estimation solution to produce a novel and highly accurate three-step procedure to solve the 3D-to-2D perspective projection pose estimation problem. Comparisons with frequently cited standard results for this problem show that our sparse adjugate-based procedure matches or exceeds the loss profiles for random simulated data sets of other known methods, which rely on more complicated iterative procedures.

Universal Least-Squares Loss Function Framework. We choose as our framework the basic least squares formulas arising when we require a set of template reference data to be rotated to agree with another set of (assumed noisy) measured data. The universal least squares loss function applicable to all of our matching problems applies an unknown rotation to the fixed reference set and compares it to a jittered test data set, and takes the following form:

$$\begin{aligned}
 S_{(2D,3D : \text{Match}, \text{Pose})} &= \sum_{k=1}^K \|R(\text{quaternion variables}) \cdot \mathbf{x}_k - \mathbf{u}_k\|^2 \\
 &= \sum_{k=1}^K \left(\mathbf{u}_k \cdot \mathbf{u}_k - 2\mathbf{u}_k \cdot R(\text{vars}) \cdot \mathbf{x}_k + \mathbf{x}_k \cdot R^t(\text{vars}) \cdot R(\text{vars}) \cdot \mathbf{x}_k \right) \\
 &= \text{tr}(U \cdot U^t) - 2 \text{tr} \left(R(\text{vars}) \cdot X \cdot U^t \right) + \text{tr} \left(R^t(\text{vars}) \cdot R(\text{vars}) \cdot X \cdot X^t \right) .
 \end{aligned} \tag{58}$$

Here $\{\mathbf{x}_k\}$ is the set of K reference points describing a cloud in dimension $D = 2$ or $D = 3$, with X denoting a $D \times K$ matrix allowing us to absorb the sums over k . We write $\{\mathbf{u}_k\}$ or U for the set of K test points. For the cloud-to-cloud matching problem, X and U denote reference data and rotated data of dimension $D = 2$ or $D = 3$, and for these same-dimension matching problems, Eq. (58) greatly simplifies due to $R^t \cdot R = \text{Identity Matrix}$, reducing the least squares minimization problem to the equivalent maximization problem for the

cross term

$$\Delta = \text{tr}(R \cdot X \cdot U^t) \quad (59)$$

after eliminating all constant terms. For the pose-estimation problem, these become a (corresponding-point-matched) projected image cloud of dimension $D = 1$ or $D = 2$, and the necessarily incomplete rotation matrices in the projection process must remain, so the full form of Eq. (58) must be retained.

There are a variety of approaches to solving each of these problems to obtain the rotation matrix that optimally aligns the two data sets X and U . We will pay particular attention to the behavior of the least squares optimization problem represented by the loss function Eq. (58) when the quaternion parameters of the rotation matrices and projections are expressed in terms of the non-singular quadratic parameterizations that we have been exploring. We will hereafter define the variables resulting from the quadratic quaternion forms as the *adjugate variables*, which we now define explicitly as:

$$\begin{aligned} \text{2D: } R(a, b) &\rightarrow R(a^2, b^2, ab) \rightarrow R(\alpha, \beta, \gamma) & P(a, b) &\rightarrow P(a^2, b^2, ab) \rightarrow P(\alpha, \beta, \gamma) \\ \text{3D: } R(q) &\rightarrow R(q_i q_j) \rightarrow R(q_{ij}) & P(q) &\rightarrow P(q_i q_j) \rightarrow P(q_{ij}) . \end{aligned} \quad (60)$$

The adjugate matrices themselves are thus given by Eq. (22) and Eq. (48), reiterated here for convenient reference:

$$\left. \begin{aligned} A(a, b) &= \begin{bmatrix} a^2 & ab \\ ab & b^2 \end{bmatrix} \equiv \begin{bmatrix} \alpha & \gamma \\ \gamma & \beta \end{bmatrix} \\ A(q) &= \begin{bmatrix} q_0^2 & q_0 q_1 & q_0 q_2 & q_0 q_3 \\ q_0 q_1 & q_1^2 & q_1 q_2 & q_1 q_3 \\ q_0 q_2 & q_1 q_2 & q_2^2 & q_2 q_3 \\ q_0 q_3 & q_1 q_3 & q_2 q_3 & q_3^2 \end{bmatrix} \equiv \begin{bmatrix} q_{00} & q_{01} & q_{02} & q_{03} \\ q_{01} & q_{11} & q_{12} & q_{13} \\ q_{02} & q_{12} & q_{11} & q_{23} \\ q_{03} & q_{13} & q_{23} & q_{33} \end{bmatrix} \end{aligned} \right\} . \quad (61)$$

While the basic mathematics is of course unchanged, the conversion from formulas quadratic or quartic in q to formulas linear or quadratic, respectively, in q_{ij} leads to some additional insights, not to speak of being explicitly nonsingular, based on the arguments in the preceding sections.

We consider applying the loss Eq. (58) here in two ways. One canonical standard for obtaining a numerical quaternion from the loss function is the *argmin* function, which takes as its input the measured data points and the unknown rotation parameters, with their constraints, which are the single equation $q \cdot q = 1$ for a pure quaternion formulation.

However, our purpose here is to add the quaternion adjugate variables to the arsenal of our analysis tools. We already are familiar with changing variables from the four unit-quaternion elements $q = (q_0, q_1, q_2, q_3)$ to their ten possible quadratic expressions written as q_{ij} , denoting variables whose behavior corresponds to $q_i \times q_j$. Since the unit-length constraint $q \cdot q = 1$ implies there are only three independent variables available, there

must be seven constraints on the ten quaternion adjugate variables q_{ij} derived from their definition. For example, $q_{00} = q_0 q_0$, $q_{11} = q_1 q_1$, and $q_{01} = q_0 q_1$ impose the constraint $q_{00} q_{11} = q_{01}^2$. While there are a number of alternative ways of extracting our needed seven constraints, we have found the following to be a universally useful combination:

$$\begin{aligned} q_{00} + q_{11} + q_{22} + q_{33} &= 1 \\ q_{00} q_{11} &= q_{01}^2, \quad q_{00} q_{22} = q_{02}^2, \quad q_{00} q_{33} = q_{03}^2 \\ q_{22} q_{33} &= q_{23}^2, \quad q_{11} q_{33} = q_{13}^2, \quad q_{11} q_{22} = q_{12}^2. \end{aligned} \tag{62}$$

This set of constraints reduces the ten adjugate variables to three independent rotation parameters, and using standard numerical constraint solution software provided in systems like Matlab or Mathematica, we get reasonable quaternion answers for noisy data in all but very unusual cases using *argmin* on the least squares loss function combined with constraints on the manifold of legal variations, e.g.,

$$\begin{aligned} \text{argmin} [& \sum_{\text{points}} \{ \| R[q] \cdot \text{reference}[x, y, z] - \text{test}[u, v, w] \|^2, \\ & q_0^2 + q_1^2 + q_2^2 + q_3^2 = 1 \}, \\ & \{ q_0, q_1, q_2, q_3 \}] \\ \\ \text{argmin} [& \sum_{\text{points}} \{ \| R[q_{ij}] \cdot \text{reference}[x, y, z] - \text{test}[u, v, w] \|^2, \\ & \{ q_{00} + q_{11} + q_{22} + q_{33} = 1, q_{00} q_{11} = q_{01}^2, q_{00} q_{22} = q_{02}^2, \\ & q_{00} q_{33} = q_{03}^2, q_{22} q_{33} = q_{23}^2, q_{11} q_{33} = q_{13}^2, q_{11} q_{22} = q_{12}^2 \}, \\ & \{ q_{00}, q_{01}, q_{02}, q_{03}, q_{11}, q_{12}, q_{13}, q_{22}, q_{23}, q_{33} \}] . \end{aligned}$$

Appropriately configured machine learning applications presumably should function identically to *argmin*. However, there are many choices to be made in designing neural networks for such purposes, and it may, for example, be challenging to reliably design an implementation, possibly leading to the observed misbehavior of such networks. We hope to deal with these issues more thoroughly in a separate venue.

Here, we will focus on a top-level overview of the ways in which quaternion adjugate variables can provide insights not only into the relationship between quaternions and rotations in numerical settings, but also into the least squares equations for point-cloud matching and their algebraic solutions. In the remaining parts of this Section, we will show how these two contexts are intimately related.

5.1 2D Point Cloud Orientation Matching

We begin with the simplest example, which we will label as “2D Matching,” namely the problem of aligning a pair of 2D point clouds, where $\{\mathbf{x}_k\} = \{[x, y]_k\}$ is a set of K 2D

column vectors describing points in a reference set, and $\{\mathbf{u}_k\} = \{[u, v]_k\}$ describes a set of 2D test points. Following our conventions in Eq. (58), the least squares loss function then takes the form

$$\mathbf{S}_{(2D \text{ Match})} = \sum_{k=1}^K \|R \cdot \mathbf{x}_k - \mathbf{u}_k\|^2. \quad (63)$$

The corresponding optimization problem is easily solved in closed form in terms of the 2×2 cross-covariance matrix

$$E_{ab} = \sum_k x_a^k u_b^k = \begin{bmatrix} x \cdot u & x \cdot v \\ y \cdot u & y \cdot v \end{bmatrix}$$

using a wide variety of methods, including quaternion forms exploiting the parameterization $R(a, b)$ (see, e.g., Hanson, 2020, supporting information, Sec. 5). We now examine what happens if we parameterize R not by the 2D quaternion itself, $q = [a, b]$, but by the adjugate-inspired variables $\{\alpha, \beta, \gamma\}$ replacing $\{a^2, b^2, ab\}$, subject to the constraints $\alpha + \beta = 1$ and $\alpha\beta = \gamma^2$. With $R(\alpha, \beta, \gamma)$, we thus find the loss function

$$\begin{aligned} \mathbf{S}_{(2D \text{ Match})} &= u \cdot u + v \cdot v - 2\alpha x \cdot u + 2\beta x \cdot u - 4\gamma x \cdot v + \alpha^2 x \cdot x + 4\gamma^2 x \cdot x - 2\alpha\beta x \cdot x + \\ &\quad \beta^2 x^2 + 4\gamma y \cdot u - 2\alpha y \cdot v + 2\beta y \cdot v + \alpha^2 y \cdot y + 4\gamma^2 y \cdot y - 2\alpha\beta y \cdot y + \beta^2 y \cdot y \\ &= u \cdot u + v \cdot v - 2\alpha x \cdot u + 2\beta x \cdot u - 4\gamma x \cdot v + 4\gamma y \cdot u - 2\alpha y \cdot v + 2\beta y \cdot v + x \cdot x + y \cdot y, \end{aligned} \quad (64)$$

where we used both constraints to remove the quaternion dependence of the $x \cdot x + y \cdot y$ terms (this is equivalent to exploiting $R \cdot R^t = I_2$ in Eq. (58)). The least squares solution minimizing \mathbf{S} in Eq. (64) is easy to find in the adjugate variable framework by using the constraints to eliminate β and γ in terms of α , requiring the derivative with respect to α to vanish, and solving the resulting quadratic equation for α . There is one subtle point, which is that, because of the form of the constraints, the relative sign of a and b (the sign of γ) can be indeterminate. Both signs give an adjugate matrix that handles the possible singularities at $[a, b] = [0, 1]$ and $[a, b] = [1, 0]$, and in fact we can determine the appropriate sign from the data, yielding a result identical with the sign-resolved quadratic products of the results from the 2D quaternion eigensystem methods noted in earlier sections.

The solution for the 2×2 adjugate matrix can be written as

$$A_{R \cdot x \rightarrow u} = \begin{bmatrix} \alpha & \gamma \\ \gamma & \beta \end{bmatrix} = \begin{bmatrix} a^2 & ab \\ ab & b^2 \end{bmatrix} = \begin{bmatrix} \frac{1}{2} \left(1 + \frac{x \cdot u + y \cdot v}{\lambda(x, y, u, v)} \right) & \frac{1}{2} \frac{x \cdot v - y \cdot u}{\lambda(x, y, u, v)} \\ \frac{1}{2} \frac{x \cdot v - y \cdot u}{\lambda(x, y, u, v)} & \frac{1}{2} \left(1 - \frac{x \cdot u + y \cdot v}{\lambda(x, y, u, v)} \right) \end{bmatrix}. \quad (65)$$

where $\lambda(x, y, u, v) = \sqrt{(x \cdot u + y \cdot v)^2 + (x \cdot v - y \cdot u)^2}$ actually turns out to be the maximal eigenvalue appearing naturally also in the quaternion matrix approach. One can easily verify that $\alpha + \beta = 1$ and $\alpha\beta = \gamma^2$. The optimal aligning 2D quaternion $[a_{\text{opt}}, b_{\text{opt}}]$ is

found as usual by identifying the maximum of α and β and normalizing its row, and the corresponding rotation matrix is $R_{\text{opt}} = R(a_{\text{opt}}, b_{\text{opt}})$. We can write the latter also in closed form as

$$R_{\text{opt}}(X, U) = \begin{bmatrix} \frac{x \cdot u + y \cdot v}{\lambda(x, y, u, v)} & -\frac{x \cdot v - y \cdot u}{\lambda(x, y, u, v)} \\ \frac{x \cdot v - y \cdot u}{\lambda(x, y, u, v)} & \frac{x \cdot u + y \cdot v}{\lambda(x, y, u, v)} \end{bmatrix}. \quad (66)$$

Equations for this problem equivalent to Eq. (66) are well-known (see, e.g., Haralick et al., 1989), but our adjugate-based derivation is novel.

5.2 2D Pose Estimation

Our next topic is the 2D pose estimation problem, “2D Pose,” which is actually a more complicated orientation problem than the 2D matching problem, even though its least squares loss function is one-dimensional and has only a single term. The problem studies the action of projections acting on 2D cloud points to obtain an image that is a line of matched points. The projection can be obtained by truncating the 2×2 rotation matrix Eq. (9) to the first line, so $P(a, b) = [a^2 - b^2, -2ab]$ or $P(\alpha, \beta, \gamma) = [\alpha - \beta, -2\gamma]$, with the adjugate matrix coordinates $\alpha = a^2$, $\beta = b^2$, $\gamma = ab$. In principle we should enforce the constraints $\alpha + \beta = 1$ and $\alpha\beta = \gamma^2$ to guarantee compatibility with the quaternion roots of our task, but it turns out that the reduced dimension of the pose estimation problem allows us some interesting additional freedom. Our least squares optimization problem takes this explicit form:

$$\mathbf{S}_{(2D \text{ Pose})} = \sum_{k=1}^K \left(P(\alpha, \beta, \gamma) \cdot [x_k, y_k]^t - u_k \right)^2 = \sum_{k=1}^K ((\alpha - \beta)x_k - 2\gamma y_k - u_k)^2 \quad (67)$$

$$= (\alpha - \beta)^2 x \cdot x - 4\gamma(\alpha - \beta) x \cdot y + 4\gamma^2 y \cdot y - 2(\alpha - \beta) x \cdot u + 4\gamma y \cdot u + u \cdot u. \quad (68)$$

Already we see something that might be interesting: while this equation is *quartic* in the quaternion (a, b) variables, making it unapproachable by the matrix methods applicable for the “2D Match” problem, it is only *quadratic* in the adjugate (α, β, γ) variables. Might it be possible to complete the squares, and get an elegant system solvable as a transformed “2D Match” problem? Unfortunately, this fails because the square completion transformation requires that the quadratic terms be represented by a symmetric nonsingular matrix (as its inverse is required), and the corresponding matrix following from Eq. (68) has *vanishing determinant*.

To exploit the reduced dimension of the adjugate parameters in the loss function Eq. (68), we proceed by requiring the vanishing of the derivatives of the loss function with respect to each variable, ignoring the constraints for the moment. We obtain three equations, but

only the following two linear equations for our three variables are independent:

$$\left. \begin{aligned} \frac{dS}{d\alpha} &= x \cdot u - \alpha x \cdot x + \beta x \cdot x + 2\gamma x \cdot y = 0 \\ \frac{dS}{d\gamma} &= y \cdot u - \alpha x \cdot y + \beta x \cdot y + 2\gamma y \cdot y = 0 \end{aligned} \right\}, \quad (69)$$

We find the partial solutions

$$\left. \begin{aligned} \alpha &= \beta + \frac{x \cdot u \ y \cdot y - y \cdot u \ x \cdot y}{x \cdot x \ y \cdot y - (x \cdot y)^2} \\ \gamma &= \frac{1}{2} \left(\frac{x \cdot u \ x \cdot y - y \cdot u \ x \cdot x}{x \cdot x \ y \cdot y - (x \cdot y)^2} \right) \end{aligned} \right\}, \quad (70)$$

At this point we are ready to use one constraint, $\alpha = 1 - \beta$, inserted into the first line of Eq. (70) to solve for β ; inserting *that* back into our equation for α , we have a complete solution in terms of only the cross-covariances: introducing the notation $\sum x_k x_k \rightarrow \text{xx}$, $\sum x_k y_k \rightarrow \text{xy}$, $\sum y_k y_k \rightarrow \text{yy}$, $\sum u_k x_k \rightarrow \text{ux}$, $\sum u_k y_k \rightarrow \text{uy}$, and $\sum u_k u_k \rightarrow \text{uu}$ for the cross-covariance sums over k , we end up with

$$\alpha = \frac{1}{2} \left(1 + \frac{\text{ux yy} - \text{uy xy}}{\text{xx yy} - \text{xy}^2} \right) \quad (71)$$

$$\beta = \frac{1}{2} \left(1 - \frac{\text{ux yy} - \text{uy xy}}{\text{xx yy} - \text{xy}^2} \right) \quad (72)$$

$$\gamma = \frac{1}{2} \frac{\text{ux xy} - \text{uy xx}}{\text{xx yy} - \text{xy}^2}. \quad (73)$$

We will find it useful to employ a notation using the 3×3 matrix of all term-by-term cross-covariance elements, including the self-covariance elements, of $[x, y]$ and $[u]$ summed over k . Accordingly, we define

$$C = \begin{bmatrix} \text{xx} & \text{xy} & \text{ux} \\ \text{xy} & \text{yy} & \text{uy} \\ \text{ux} & \text{uy} & \text{uu} \end{bmatrix}. \quad (74)$$

Our algebraic solutions reduce to ratios of 2×2 subdeterminants of Eq. (74), which we choose to write using the notation

$$d_1 \rightarrow \begin{bmatrix} \text{xx} & \text{xy} \\ \text{xy} & \text{yy} \end{bmatrix} \quad d_2 \rightarrow \begin{bmatrix} \text{ux} & \text{xy} \\ \text{uy} & \text{yy} \end{bmatrix} \quad d_3 \rightarrow \begin{bmatrix} \text{ux} & \text{xx} \\ \text{uy} & \text{xy} \end{bmatrix} \quad (75)$$

Thus

$$\alpha = \frac{1}{2} \left(1 + \frac{d_2}{d_1} \right) \quad \beta = \frac{1}{2} \left(1 - \frac{d_2}{d_1} \right) \quad \gamma = \frac{1}{2} \frac{d_3}{d_1} \quad (76)$$

To complete our solution of the 2D Pose problem, we note that while Eqs. (76) satisfy the constraints $\alpha + \beta = 1$, they do not satisfy our second constraint $\alpha\beta = \gamma^2$. However, it is important to remember that there is one less matrix element in the loss function Eq. (67) than a full rotation matrix loss. If we attempt to construct the projection, that is the top line of the 2D rotation matrix, and insert the solutions Eq. (76), we find the following approximate first step, which in fact gives perfect solutions for noise-free test data:

$$\begin{aligned} \tilde{P}(\alpha, \beta, \gamma) &= [\alpha - \beta, \quad -2\gamma] \\ &= \left[\frac{(u \cdot x \ y \cdot y - u \cdot y \ x \cdot y)}{x \cdot x \ y \cdot y - (x \cdot y)^2}, \quad \frac{(u \cdot y \ x \cdot x - u \cdot x \ x \cdot y)}{x \cdot x \ y \cdot y - (x \cdot y)^2} \right] \\ &= \left[\frac{d_2}{d_1}, -\frac{d_3}{d_1} \right] \end{aligned} \quad (77)$$

Evaluating this tentatively as the projection in the 2D Pose loss function, Eq. (67), against an arbitrary list of pure or noisy data sets, we find that even though its scale varies through a range near unity, unlike a rotation matrix row, it still scores very well as a target for a minimizer of Eq. (67). Remarkably, without doing any further computation, but simply normalizing Eq. (77) to produce a legal partial rotation matrix element, results in mean losses of $\approx 10^{-30}$ for pure data, and mean losses smaller than those using the *known* initial value for the 2D projection Eq. (77). Combining the projection matrix element Eq. (77) with its orthogonal partner (the 2D cross-product) and normalizing produces a perfect orthogonal rotation matrix, which is the solution to the 2D Pose least squares problem:

$$\begin{aligned} R(\alpha, \beta, \gamma) &= \left[\frac{\begin{bmatrix} (u \cdot x \ y \cdot y - u \cdot y \ x \cdot y) & (u \cdot y \ x \cdot x - u \cdot x \ x \cdot y) \\ (u \cdot x \ x \cdot y - u \cdot y \ x \cdot x) & (u \cdot x \ y \cdot y - u \cdot y \ x \cdot y) \end{bmatrix}}{((u \cdot x \ y \cdot y - u \cdot y \ x \cdot y)^2 + (u \cdot y \ x \cdot x - u \cdot x \ x \cdot y)^2)^{1/2}} \right] \\ &= \frac{1}{\sqrt{d_2^2 + d_3^2}} \begin{bmatrix} d_2 & -d_3 \\ d_3 & d_2 \end{bmatrix}. \end{aligned} \quad (78)$$

Remark: We will see in the 3D pose problem that, to handle noisy data that move the least squares solution away from a pure rotation, we will take one more step: the transition from the projection-matrix solution that works for noise-free data to a full rotation matrix that preserves its form for noisy data will require applying the Bar-Itzhack procedure to find the *optimal* pure rotation matrix given an approximate candidate. The 2D case has much less structure, and can avoid that complication. One can check that applying the Bar-Itzhack process to the numerator of Eq. (78) produces exactly the same rotation matrix.

In Fig. (4), we show that $R(\alpha, \beta, \gamma)$ in Eq. (78) is indeed an exact rotation matrix giving the relation between an initial point cloud $[x, y]$ and its projection $[u]$ after a rotation and added noise. We show that it outperforms the rotation that was used to simulate the pose data (referred to as *rot_mat*); this should be very good, but somewhat random and less

deterministic than the least squares solution, since it has *no way of knowing* what the least squares formula is.

Final remarks on the 2D Pose least squares problem. The fact that Eq. (77) satisfies both constraints and achieves basically vanishing loss for perfect data was somewhat unexpected, but is very likely related to the fact that the eigenvalues for the quaternion profile matrix approach to solving the “Match” class of problems are rotation-invariant; this feature is maintained in all the numerical experiments we have done, and presumably there is a direct proof related to our invariance proof for the “Match” problem in Appendix B. The literature on the subject of pose estimation contains numerous papers mentioning closed form solutions and good approximation methods, but typically the exact solutions are lists of alternative roots of equations that must be evaluated one by one against the loss function, and, in the end, numerical optimization methods such as Newton’s method or neural networks are often preferred to achieve experimental results (see, e.g., Haralick et al., 1989; Olsson et al., 2006; Wientapper and Kuijper, 2016; Wientapper et al., 2018; Wientapper and Kuijper, 2016; Zhou et al., 2020). In 2D, the simple least squares solution Eq. (78) that we found can undoubtedly be obtained by any of many equivalent methods; however, our derivation based on the quaternion adjugate matrix provides a clear picture of what is happening. The key is that rotation parameterizations are subtle structures, even in 2D, as we saw in Section 3. There are several fundamental insights that appear: one is that if you drop one line of a rotation matrix to produce a projection matrix, there is still enough information present to reproduce the full $N \times N$ rotation matrix by simply taking the cross-product of the lines of the projection matrix to find the missing line. Next is that both the algebraic methods to extract a least-squares solution from a squared-difference loss function such as Eq. (67) and the numerical methods such as *argmin* methods produce answers without anomalies *only if the correct, reduced, number of constraints is imposed*; what we found was that for the 2D Match problem, both the constraints must be applied, but for the 2D Pose problem, only the first constraint is necessary, in addition to normalization, and in fact one gets excessive ambiguous branched solutions otherwise (we will see a similar thing in the 3D Pose problem later). Finally, the particular constraints that are successful in guiding *argmin* include, for example, the *topological constraints on orthonormality of the rows of the projection matrix*, which for 2D are simply $\alpha + \beta = 1$ plus the one-line normalization. These are the key observations; we conjecture that any successful pose estimation problem has these properties, which are clarified by formulating the problem using quaternion adjugate variables to parameterize the rotation, which is computed *directly*, without going through an isolated quaternion stage. We conclude by noting that *if* a quaternion is desired, which can often be the case if one wants to visualize global features of families of rotations, the quaternion can be at once extracted using the fundamental methods such as the Bar-Itzhack optimization described in Sections 3 and 4.

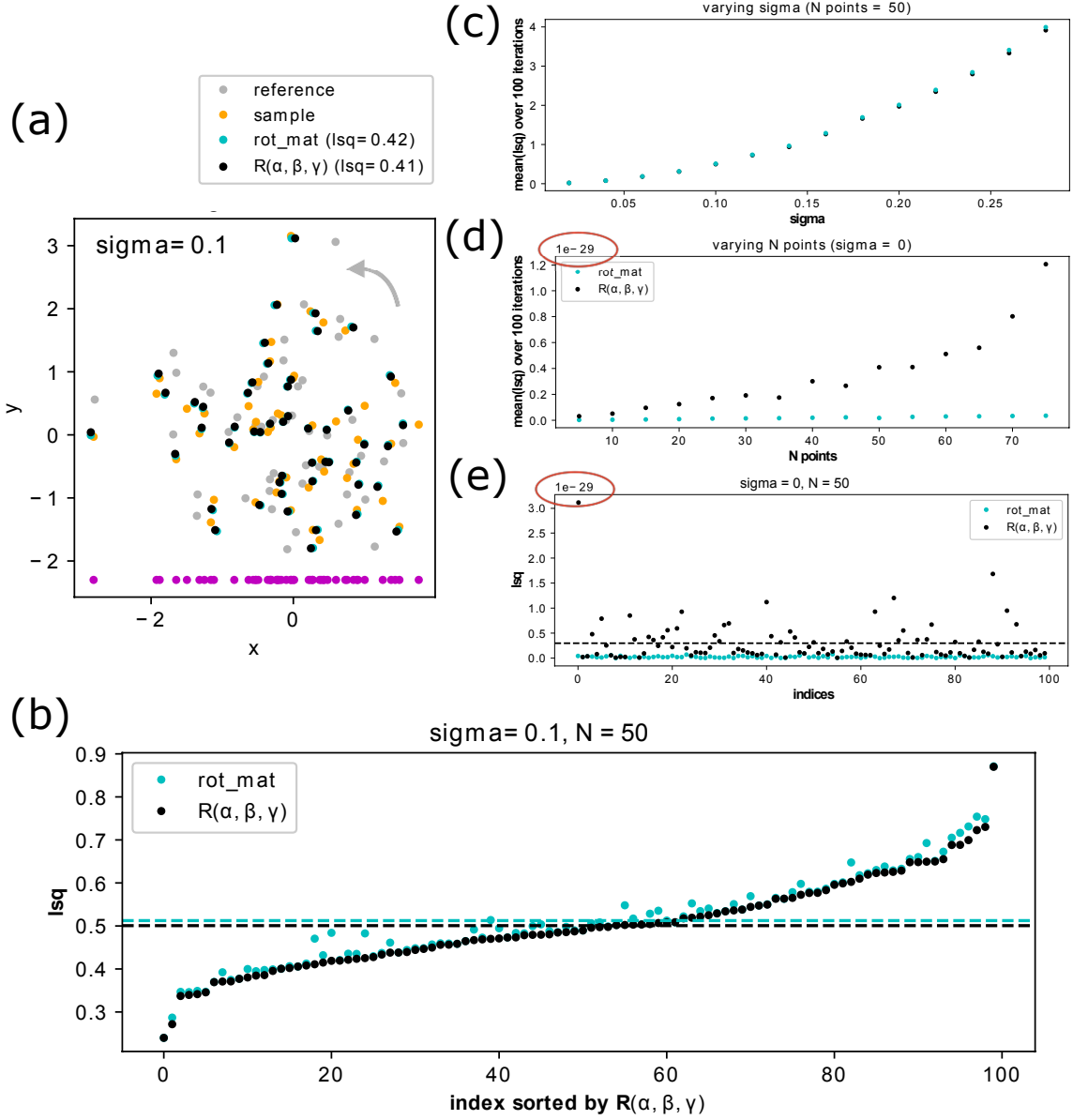


Figure 4: **Results using Analytical Solution to the 2D Point-Cloud Projection Problem.** (a) Example data for a small rotation with noise $\sigma = 0.1$: original reference data in grey, rotated sample points in orange, points using rotation matrix without noise in cyan (mostly hidden), results using our analytical solution $R(\alpha, \beta, \gamma)$ in black, and projected points in magenta. (b) Comparison of least squared errors between our analytical solution $R(\alpha, \beta, \gamma)$ and the original rot_mat for 100 random 2D point clouds with $N = 50$ and $\sigma = 0.1$. Data are sorted by the $R(\alpha, \beta, \gamma)$ results, and dashed lines indicate the mean. (c) Exploration of the dependency of the least squared errors on σ , here with $N = 50$, and we plot the mean results over 100 iterations. The coloring is as in (b). (d,e) Exploring the no-noise case for $R(\alpha, \beta, \gamma)$: The original rot_mat performs consistently better, especially as the number of points N in the cloud increases; one set of 100 iterations with $N = 50$ is shown for clarity. In both cases note that the scale of the y axis is 10^{-29} .

5.3 3D Point-Cloud Matching

Moving on to 3D data, we consider first the classic “3D Match” problem, also known as the RMSD or “Generalized Procrustes” problem, whose task is to find the 3D rotation best aligning a possibly noisy test cloud with a reference cloud to which it corresponds. As noted, here we choose a least squares loss function for our purposes that reverses the common order and applies the rotation matrix to align the reference cloud with the test cloud. We assume we have two 3D point clouds of size K , a reference set $\{\mathbf{x}_k\} = \{[x, y, z]_k\}$ that we consider as a list of K columns of 3D points, and a test set of noisy measured 3D points $\{\mathbf{u}_k\} = \{[u, v, w]_k\}$ that is believed to be related, pointwise, to the reference set by an unknown rotation. If we choose to express that rotation using Eq. (1) as $R(q)$, then we can write the least-squares optimization target as (see, e.g., Horn, 1987; Hanson, 2020).

$$\mathbf{S}_{(3D \text{ Match})}(q) = \sum_{k=1}^K \|R(q) \cdot \mathbf{x}_k - \mathbf{u}_k\|^2. \quad (79)$$

There are well-known procedures using quaternion eigensystems to solve this problem in closed form either from the least squares functional $\mathbf{S}(q)$ (see Faugeras and Hebert (1983, 1986)), or from the cross-term, which reduces to a trace over the rotated 3×3 cross-covariance matrix E_{ab} (see, e.g., Horn, 1987),

$$\Delta(q) = \text{tr } R(q) \cdot (X \cdot U^t) = \text{tr } R(q) \cdot E. \quad (80)$$

Because the $R^t \cdot R$ factor in Eq. (79) disappears from this least squares optimization function, we can always express the problem of finding the optimal quaternion using a *quadratic* function of quaternions, and the problem is solvable using standard linear algebra. (Non-quaternion methods such as SVD are also widely used.) We reiterate that in the 3D→2D pose-estimation problem to be dealt with in the next subsection, those terms no longer cancel, and the expression for $\mathbf{S}(q)$ becomes *quartic* in q , and Eq. (80) is no longer applicable.

The Adjugate. We now explore how the adjugate variables can be incorporated into this problem. Starting from the standard framework of Eq. (79), we see there is little motivation to use the full $\mathbf{S}(q)$ form, since all the quartic terms disappear, and only the non-constant cross-term $\Delta(q)$ shown in Eq. (80) is relevant. In the standard quaternion solution of the optimal rotation problem, we rearrange the cross-term into a form that is optimized by the maximal eigenvector of the profile matrix, $M(E)$ (see, e.g., Hanson (2020) for further references and a review). We find

$$\Delta(q) = \text{tr } R(q) \cdot E = (q_0, q_1, q_2, q_3) \cdot M(E) \cdot (q_0, q_1, q_2, q_3)^t \equiv q \cdot M(E) \cdot q, \quad (81)$$

where $M(E)$ is the traceless, symmetric 4×4 matrix that is composed of linear functions of the elements of the 3×3 cross-covariance matrix $E = X \cdot U^t$ of the data:

$$M(E) = \begin{bmatrix} E_{xx} + E_{yy} + E_{zz} & E_{yz} - E_{zy} & E_{zx} - E_{xz} & E_{xy} - E_{yx} \\ E_{yz} - E_{zy} & E_{xx} - E_{yy} - E_{zz} & E_{xy} + E_{yx} & E_{zx} + E_{xz} \\ E_{zx} - E_{xz} & E_{xy} + E_{yx} & -E_{xx} + E_{yy} - E_{zz} & E_{yz} + E_{zy} \\ E_{xy} - E_{yx} & E_{zx} + E_{xz} & E_{yz} + E_{zy} & -E_{xx} - E_{yy} + E_{zz} \end{bmatrix}. \quad (82)$$

In the usual method, the transformed loss function Eq. (81), now a maximization problem, is solved by computing the maximal eigenvalue λ_{opt} of $M(E)$, and identifying its normalized eigenvector as exactly q_{opt} , with $R_{\text{opt}} = R(q_{\text{opt}})$ solving the matching problem. However, in every such calculation, there is an often-hidden step that relates precisely to one of our main points in this paper: there are *always* fourteen submanifolds of possible quaternion solutions that can obstruct obtaining a normalizable quaternion from $M(E)$ and λ_{opt} ! These are avoided by scaling one element of the unknown eigenvector to unity, and solving the eigenvector equation for the three remaining elements using Kramer's rule; if that eigenvector element happens to vanish, this fails, and one sets the *next* element to unity, repeating until successful. Whatever methods a library eigensystem program uses to return a valid eigenvector of this system corresponding to the maximal eigenvalue of $M(E)$, it will always be exactly equivalent to computing the characteristic matrix and its adjugate,

$$\begin{aligned} \chi(E) &= [M(E) - \lambda_{\text{opt}} I_4] \\ A(E) &= \text{Adjugate}(\chi(E)) , \end{aligned}$$

finding the maximum-magnitude diagonal of $A(E)$, and normalizing that row to guarantee the computation will not encounter one of the singular domains of unnormalizable eigenvectors.

For our purposes, we now rephrase the 3D Match problem to employ the quaternion adjugate variables $q_{ij} = q_i q_j$ instead of the quaternions q_i themselves. Then, with $R(q)$'s quadratic form in q replaced by the adjugate form

$$R(q_{ij}) = \begin{bmatrix} q_{00} + q_{11} - q_{22} - q_{33} & 2q_{12} - 2q_{03} & 2q_{13} + 2q_{02} \\ 2q_{12} + 2q_{03} & q_{00} - q_{11} + q_{22} - q_{33} & 2q_{23} - 2q_{01} \\ 2q_{13} - 2q_{02} & 2q_{23} + 2q_{01} & q_{00} - q_{11} - q_{22} + q_{33} \end{bmatrix} , \quad (83)$$

we find that $\Delta(q_{ij})$ now defines a superficially *linear* optimization problem, in ten dimensions, that takes the form

$$\Delta(q_{ij}) = \text{tr } R(q_{ij}) \cdot E = \sum_{i \leq j} q_{ij} M(E)_{ij} . \quad (84)$$

If all the q_{ij} were independent up to an overall scale, the solution $q_{ij} \propto M_{ij}$ would immediately be seen to maximize Δ . This opportunity is unfortunately obstructed by the

fact that the ten adjugate variables are not independent, but are related by the seven constraints of Eq. (62) that reduce the superficial problem in ten free variables down to the required three parameters of 3D rotations.

We can now recast the problem traditionally solved using the maximal eigenvalue of $M(E)$ and its associated normalized eigenvector, which is just q_{opt} , in several ways. First, we can simply use Eq. (62) to reduce all the ten q_{ij} to functions of just three independent adjugate variables such as (q_{11}, q_{22}, q_{33}) , and require that all three corresponding derivatives of Eq. (84) vanish. This is an effective solution with the drawback that there are eight alternative sign-permuted solutions due to the square roots in the constraint equations, and the correct values of (q_{11}, q_{22}, q_{33}) appear in only one of these terms for any data set, and which term that is appears to be indeterminate. In addition, the signs of the remaining seven terms in the list of adjugate variables are indeterminate as well. The correct adjugate matrix can always be found by checking all permutations substituted into the optimization function Eq. (84) and using the choices giving the maximal value, but that is an awkward algorithm compared to the maximal quaternion eigensystem method.

We note one other alternative approach that can be used, driven by the proof in Appendix B that for *error-free data*, the maximal eigenvalue of $M(E)$ is independent of $R(q)$. Thus the maximal eigenvalue is the same as the maximal eigenvalue of $M(E_0)$, where $E_0 = X \cdot X^t$ is the self-covariance of the reference data, and that value is simply

$$\lambda_{\text{opt}} = \text{tr } E_0 . \quad (85)$$

A candidate quaternion applicable to error-free data thus emerges from the hybrid characteristic equation

$$\chi(E, E_0) = [M(E) - \text{tr}(E_0)I_4]$$

upon computing the adjugate,

$$A(\chi) = \text{Adjugate}(\chi(E, E_0)) ,$$

and computing the optimal quaternion q_{opt} from the largest-magnitude row of $A(\chi)$. For noise-containing data, the procedure becomes somewhat circular for the particular task of 3D cloud-matching, as the rotation $R_{\text{opt}} = R(q_{\text{opt}})$ becomes inexact, and one unavoidably has to compute a more complicated maximal eigenvalue to solve the Bar-Itzhack problem, producing an optimal exact rotation matrix $R_{\text{BI}} \approx R(q_{\text{opt}})$ that produces an acceptable solution to the 3D cloud matching problem.

5.4 3D to 2D Pose Estimation

Finally, we turn our attention to the “3D Pose” pose-estimation problem that corresponds most closely to the classic 3D RMSD squared-difference optimization. We suppose we

have a 3D point cloud reference set X that we consider as a list of K columns of 3D points $\{\mathbf{x}_k\}$, and a 2D test set of points U , with 2D image-plane components $\{\mathbf{u}_k\}$ that are considered as paired images of each point in the 3D cloud projected in parallel from some to-be-determined camera orientation. Here we study only the idealized case of the parallel projection described by a 2×3 projection matrix $P(q)$ that is extracted from the top two rows of a 3D rotation matrix; this is of course quite relevant for applications like microscopy for which the effective focal length relative to the scale of the data is infinite.

If we choose to express our rotation using Eq. (1) as $R(q)$, then we may write the projection as

$$P(q) = \begin{bmatrix} q_0^2 + q_1^2 - q_2^2 - q_3^2 & 2q_1q_2 - 2q_0q_3 & 2q_1q_3 + 2q_0q_2 \\ 2q_1q_2 + 2q_0q_3 & q_0^2 - q_1^2 + q_2^2 - q_3^2 & 2q_2q_3 - 2q_0q_1 \end{bmatrix}, \quad (86)$$

and the least-squares optimization target can be written

$$\mathbf{S}_{\text{3D Pose}} = \sum_{k=1}^K \|P(q) \cdot \mathbf{x}_k - \mathbf{u}_k\|^2. \quad (87)$$

While the 3D point cloud matching loss function in Section 5.3 can be reduced to the quadratic cross-term Δ and solved using an optimal quaternion eigenvector, *this approach fails for pose estimation*. In the pose-estimation problem we can no longer eliminate the quartic quaternion part of the optimization and the problem becomes potentially much more complex.

The adjugate formalism now comes into play: we replace the individual quaternions in Eq. (87), as they appear in Eq. (86), by their adjugate quadratic forms, $q_i q_j \rightarrow q_{ij}$, so our adjugate-valued projection matrix becomes

$$P(q_{ij}) = \begin{bmatrix} q_{00} + q_{11} - q_{22} - q_{33} & 2q_{12} - 2q_{03} & 2q_{13} + 2q_{02} \\ 2q_{12} + 2q_{03} & q_{00} - q_{11} + q_{22} - q_{33} & 2q_{23} - 2q_{01} \end{bmatrix}. \quad (88)$$

We note the projection matrix is lacking these matrix elements, $q_{13} - q_{02}$, $q_{23} + q_{01}$, and $q_{00} - q_{11} - q_{22} + q_{33}$, so the number of constraints needed can in principle be reduced. Secondly, those variables are in a specific sense recoverable because, since $P(q_{ij})$ is part of an orthonormal 3×3 matrix, the missing bottom row can be computed, if the first two rows have been determined, by taking the cross-product of the two rows of $P(q_{ij})_{\text{opt}}$ and normalizing the result (if necessary) to get the missing last row of a full orthonormal rotation matrix. The resulting form of Eq. (87) now becomes a quadratic function in the adjugate variables q_{ij} that can be solved, in principle, using least squares algebraic methods, resulting in a computable adjugate matrix from which a guaranteed non-singular quaternion can be extracted. Our loss function, written in terms of the measured data components summed over K , is complicated by the appearance of both linear and quadratic terms in

q_{ij} , and takes the form:

$$\begin{aligned}
\mathbf{S}_{3D \text{ Pose}}(q_{ij}, x, y, z, u, v) = & \\
& q_{00}^2 x \cdot x + q_{11}^2 x \cdot x + q_{22}^2 x \cdot x + q_{33}^2 x \cdot x + q_{00}^2 y \cdot y + q_{11}^2 y \cdot y + q_{22}^2 y \cdot y + q_{33}^2 y \cdot y \\
& - 4q_{00}q_{01} y \cdot z + 4q_{00}q_{02} x \cdot z + 2q_{00}q_{11} x \cdot x - 2q_{00}q_{11} y \cdot y + 8q_{00}q_{12} x \cdot y \\
& + 4q_{00}q_{13} x \cdot z - 2q_{00}q_{22} x \cdot x + 2q_{00}q_{22} y \cdot y + 4q_{00}q_{23} y \cdot z - 2q_{00}q_{33} x \cdot x - 2q_{00}q_{33} y \cdot y \\
& - 2q_{00} u \cdot x - 2q_{00} v \cdot y + 4q_{01}^2 z \cdot z - 8q_{01}q_{03} x \cdot z + 4q_{01}q_{11} y \cdot z - 8q_{01}q_{12} x \cdot z \\
& - 4q_{01}q_{22} y \cdot z - 8q_{01}q_{23} z \cdot z + 4q_{01}q_{33} y \cdot z + 4q_{01} v \cdot z + 4q_{02}^2 z \cdot z - 8q_{02}q_{03} y \cdot z \\
& + 4q_{02}q_{11} x \cdot z + 8q_{02}q_{12} y \cdot z + 8q_{02}q_{13} z \cdot z - 4q_{02}q_{22} x \cdot z - 4q_{02}q_{33} x \cdot z - 4q_{02} u \cdot z \\
& + 4q_{03}^2 x \cdot x + 4q_{03}^2 y \cdot y - 8q_{03}q_{11} x \cdot y + 8q_{03}q_{12} x \cdot x - 8q_{03}q_{12} y \cdot y - 8q_{03}q_{13} y \cdot z \\
& + 8q_{03}q_{22} x \cdot y + 8q_{03}q_{23} x \cdot z + 4q_{03} u \cdot y - 4q_{03} v \cdot x + 4q_{11}q_{13} x \cdot z - 2q_{11}q_{22} x \cdot x \\
& - 2q_{11}q_{22} y \cdot y - 4q_{11}q_{23} y \cdot z - 2q_{11}q_{33} x \cdot x + 2q_{11}q_{33} y \cdot y - 2q_{11} u \cdot x + 2q_{11} v \cdot y \\
& + 4q_{12}^2 x \cdot x + 4q_{12}^2 y \cdot y + 8q_{12}q_{13} y \cdot z + 8q_{12}q_{23} x \cdot z - 8q_{12}q_{33} x \cdot y - 4q_{12} u \cdot y \\
& - 4q_{12} v \cdot x + 4q_{13}^2 z \cdot z - 4q_{13}q_{22} x \cdot z - 4q_{13}q_{33} x \cdot z - 4q_{13} u \cdot z + 4q_{22}q_{23} y \cdot z \\
& + 2q_{22}q_{33} x \cdot x - 2q_{22}q_{33} y \cdot y + 2q_{22} u \cdot x - 2q_{22} v \cdot y + 4q_{23}^2 z \cdot z - 4q_{23}q_{33} y \cdot z \\
& - 4q_{23} v \cdot z + 2q_{33} u \cdot x + 2q_{33} v \cdot y + u \cdot u + v \cdot v .
\end{aligned} \tag{89}$$

(Note that it is the sum of q_{ii} that sums to unity, not the sum of q_{ii}^2 , so there is no simplification in the first line.) Parallel to the 2D case, one cannot complete the squares to recover a simpler quadratic form in a transformed variable set because the 10×10 matrix incorporating the quadratic products of the adjugate variables is singular. As usual, the redundancy of the adjugate variables has to be reduced by the imposition of constraints such as those in Eq. (62). However, we are potentially lacking some degrees of freedom in the projection-matrix adjugate variables, so if we try to constrain all the variables, we may come up with no solutions. Thus it appears possible that we do not need (or cannot utilize) all seven adjugate constraints in order to obtain the canonical three rotational degrees of freedom in a rotation.

5.4.1 Solving the 3D Pose Least-Squares Loss Function Algebraically

We can get full solutions of the least squares problem defined by the general form of Eq. (63) using a specific choice of the adjugate constraints in Eq. (62). When we impose the four constraints containing the adjugate variable q_{00} , with `lossRPOSE3DAdj` denoting the algebraic expression Eq. (89) and symbols for the cross-covariance terms $x \cdot y$ and etc., this Mathematica expression yields a list of eight candidate solutions:

```

the3D2DAdjSolns =
Module[{eqn = lossPose3DAdj},

```

```

Solve[ { D[eqn, q00] == 0,
        D[eqn, q11] == 0, D[eqn, q22] == 0, D[eqn, q33] == 0,
        D[eqn, q01] == 0, D[eqn, q02] == 0, D[eqn, q03] == 0,
        D[eqn, q23] == 0, D[eqn, q13] == 0, D[eqn, q12] == 0,
        q00 + q11 + q22 + q33 == 1,
        q00 q11 == q01 q01, q00 q22 == q02 q02, q00 q33 == q03 q03
(* q22 q33==q23 q23,q11 q33==q13 q13,q11 q22==q12 q12 *) },
{q00, q11, q22, q33, q01, q02, q03, q23, q13, q12}]] .

```

(The three unused constraints are commented out, retained for later reference.) The resulting set of eight algebraic expressions can be tested by substituting randomly generated rotations applied to a cloud of points, and adding noise to generate a 2D projected data image. We test each of the list of 8 against 100 data sets to see, first, whether they produce an adjugate matrix that provides a solution, and then to see whether the resulting solutions obey all seven constraints in Eq. (62). For exact data, four of the solutions are usually complex, and thus unusable. Four of the solutions are always real, and, strangely, exactly *one* of them always produces the quaternion (via the adjugate procedure) that was used to generate the data. However, we have more work to do to achieve a deterministic algorithm. For pure data, all the constraints are in fact obeyed, while for errorful data, the constraint identities that were *enforced* are always maintained, while those that were not enforced (commented out in the `the3D2DAdjSolns` expression) are no longer valid. We can do better, but first we need some notation, as the immediate algebraic solutions in some cases are ten megabytes in length.

We have found a useful symbolic representation of the first four solutions, one of which always gives the right quaternion for error-free data sets. We introduce first the 5×5 matrix of all term-by-term cross-covariance elements, including the self-covariance elements, of $[x, y, z]$ and $[u, v]$ summed over k , denoting $\sum x_k x_k \rightarrow xx$, $\sum x_k y_k \rightarrow xy$, \dots , $\sum z_k v_k \rightarrow vz$, so we have

$$C = \begin{bmatrix} xx & xy & xz & ux & vx \\ xy & yy & yz & uy & vy \\ xz & yz & zz & uz & vz \\ ux & uy & uz & uu & uv \\ vx & vy & vz & uv & vv \end{bmatrix}. \quad (90)$$

All of the algebraic solutions reduce to ratios of order 3 products of the elements of cross-covariances Eq. (90) or square roots of appropriate powers of such elements. We define the

3×3 subdeterminants of Eq. (90) using the notation

$$\begin{aligned}
d_1 &\rightarrow \begin{bmatrix} \text{xx} & \text{xy} & \text{xz} \\ \text{xy} & \text{yy} & \text{yz} \\ \text{xz} & \text{yz} & \text{zz} \end{bmatrix} \\
d_2 &\rightarrow \begin{bmatrix} \text{xx} & \text{xy} & \text{ux} \\ \text{xy} & \text{yy} & \text{uy} \\ \text{xz} & \text{yz} & \text{uz} \end{bmatrix} \quad d_3 \rightarrow \begin{bmatrix} \text{xx} & \text{xy} & \text{vx} \\ \text{xy} & \text{yy} & \text{vy} \\ \text{xz} & \text{yz} & \text{vz} \end{bmatrix} \quad d_4 \rightarrow \begin{bmatrix} \text{xx} & \text{xz} & \text{ux} \\ \text{xy} & \text{yz} & \text{uy} \\ \text{xz} & \text{zz} & \text{uz} \end{bmatrix} \\
d_5 &\rightarrow \begin{bmatrix} \text{xx} & \text{xz} & \text{vx} \\ \text{xy} & \text{yz} & \text{vy} \\ \text{xz} & \text{zz} & \text{vz} \end{bmatrix} \quad d_6 \rightarrow \begin{bmatrix} \text{xx} & \text{ux} & \text{vx} \\ \text{xy} & \text{uy} & \text{vy} \\ \text{xz} & \text{uz} & \text{vz} \end{bmatrix} \quad d_7 \rightarrow \begin{bmatrix} \text{xy} & \text{xz} & \text{ux} \\ \text{yy} & \text{yz} & \text{uy} \\ \text{yz} & \text{zz} & \text{uz} \end{bmatrix} \\
d_8 &\rightarrow \begin{bmatrix} \text{xy} & \text{xz} & \text{vx} \\ \text{yy} & \text{yz} & \text{vy} \\ \text{yz} & \text{zz} & \text{vz} \end{bmatrix} \quad d_9 \rightarrow \begin{bmatrix} \text{xy} & \text{ux} & \text{vx} \\ \text{yy} & \text{uy} & \text{vy} \\ \text{yz} & \text{uz} & \text{vz} \end{bmatrix} \quad d_{10} \rightarrow \begin{bmatrix} \text{xz} & \text{ux} & \text{vx} \\ \text{yz} & \text{uy} & \text{vy} \\ \text{zz} & \text{uz} & \text{vz} \end{bmatrix},
\end{aligned} \tag{91}$$

where d_1 plays a special role as the *self-covariance* of the reference cloud's point values. The four usable versions of the least-squares solutions differ by pairs of signs of square roots in the expressions for $(q_{01}, q_{02}, q_{23}, q_{13})$, so we can write the 3D pose least squares solutions as a function of their corresponding square root signs, which we denote by s_{ij} . We can then express the four solutions in terms of the combinations of signs that distinguish one from another as $\omega(s_{01}, s_{02}, s_{23}, s_{13})$, where

$$\left. \begin{aligned} \text{soln}(1) &= \omega(+1, +1; +1, +1) \\ \text{soln}(2) &= \omega(+1, -1; +1, -1) \\ \text{soln}(3) &= \omega(-1, +1; -1, +1) \\ \text{soln}(4) &= \omega(-1, -1; -1, -1) \end{aligned} \right\}. \tag{92}$$

Then a more explicit form of the solutions terms of the cross-covariance determinants of

Eq. (91) takes the form

$$\omega(s_{01}, s_{02}, s_{23}, s_{13}) = \left[\begin{array}{l} q_{00} \rightarrow \frac{\sqrt{d_1^2(-d_4+(d_5-d_7)^2-d_8)}+d_1(d_7-d_5)}{4d_1^2} \\ q_{11} \rightarrow \frac{d_1(2d_1+d_5+d_7)-\sqrt{d_1^2(-d_4+(d_5-d_7)^2-d_8)}}{4d_1^2} \\ q_{22} \rightarrow -\frac{\sqrt{d_1^2(-d_4+(d_5-d_7)^2-d_8)}+d_1(-2d_1+d_5+d_7)}{4d_1^2} \\ q_{33} \rightarrow \frac{\sqrt{d_1^2(-d_4+(d_5-d_7)^2-d_8)}+d_1(d_5-d_7)}{4d_1^2} \\ q_{01} \rightarrow -\frac{s_{01}\sqrt{2(d_1+d_5)\left(\sqrt{d_1^2(-d_4+(d_5-d_7)^2-d_8)}+d_1(d_7-d_5)\right)}-d_1(d_4+d_8)^2}{4\sqrt{d_1^3}} \\ q_{02} \rightarrow -\frac{s_{02}\sqrt{2(d_1-d_7)\left(\sqrt{d_1^2(-d_4+(d_5-d_7)^2-d_8)}+d_1(d_7-d_5)\right)}-d_1(d_4+d_8)^2}{4\sqrt{d_1^3}} \\ q_{03} \rightarrow \frac{d_4+d_8}{4d_1} \\ q_{23} \rightarrow \frac{d_3}{2d_1} - \frac{s_{23}\sqrt{2(d_1+d_5)\left(\sqrt{d_1^2(-d_4+(d_5-d_7)^2-d_8)}+d_1(d_7-d_5)\right)}-d_1(d_4+d_8)^2}{4\sqrt{d_1^3}} \\ q_{13} \rightarrow \frac{d_2}{2d_1} + \frac{s_{13}\sqrt{2(d_1-d_7)\left(\sqrt{d_1^2(-d_4+(d_5-d_7)^2-d_8)}+d_1(d_7-d_5)\right)}-d_1(d_4+d_8)^2}{4\sqrt{d_1^3}} \\ q_{12} \rightarrow \frac{d_8-d_4}{4d_1} \end{array} \right] \quad (93)$$

With careful examination and experimentation, the daunting form of Eq. (93) reveals some remarkable structure. If one takes a list of error-free data sets, and, evaluates all four functions in Eq. (93) *against the pose loss function* Eq. (89), all four least-squares alternate solutions produce a *perfect match*. This seems impossible until one carefully checks the steps, and discovers that, although the elements (q_{01} , q_{02} , q_{23} , q_{13}) differ among the four functions, when all are combined together to form the 2×3 *projection matrix* $P(q_{ij})$, the *differences cancel and all four produce the same projection with no square roots*.

Since only the top two lines enter into the least squares loss formula, this is completely logical: our solution only asks to minimize those two lines, and the third line does not appear at all, and in fact if we substitute the four versions of q_{ij} solutions in Eq. (93) into the third line of the adjugate-parameterized rotation matrix Eq. (83), they are *all different*. Now we come to a procedure that remarkably takes us full circle back to the calculations for optimal matches to noisy rotation matrices in Section 4.3. First, since we get a perfect first two lines of the rotation matrix for all four solutions, we can simply construct the third line by taking the cross-product of the two projection-matrix components. In the second step, we observe that for noisy test data, the perfect success of Eq. (93) is deformed and, in

general, we do not know exactly what process is going on. However, the basic fact is that what we need is an optimal rotation matrix that is the *ideal* approximation, with perfect orthonormality, to our solution that (so far) behaves well only for perfect data. We already know how to do that, from our work in previous sections on extracting adjugate vectors, and hence quaternions, using methods like those in the introductory sections.

For pedagogical reasons that will become clear, we first write the initial form of the projection-matrix solution in terms of the cross-covariance determinants in Eq. (91) as follows:

$$\tilde{P}(x, y, z; u, v) = \begin{bmatrix} \frac{d_7}{d_1} & -\frac{d_4}{d_1} & \frac{d_2}{d_1} \\ \frac{d_8}{d_1} & -\frac{d_5}{d_1} & \frac{d_3}{d_1} \end{bmatrix}. \quad (94)$$

On any error-free data set, this projection remarkably is a perfect least-squares solution, is orthonormal, and produces a vanishing loss function to 30 orders of magnitude accuracy. If we ignore the disagreements with the form of the third rotation-matrix line coming from the four solutions for q_{ij} , we can simply take the cross-product of the two lines, that is $P_1 \times P_2$, and that will give a unique answer for a third line that will also be orthonormal on pure data, establishing our initial form for the full 3D Pose rotation matrix solution of the form

$$\tilde{R}(x, y, z; u, v) = \begin{bmatrix} \frac{d_7}{d_1} & -\frac{d_4}{d_1} & \frac{d_2}{d_1} \\ \frac{d_8}{d_1} & -\frac{d_5}{d_1} & \frac{d_3}{d_1} \\ \frac{d_6}{d_1} & \frac{d_9}{d_1} & \frac{d_{10}}{d_1} \end{bmatrix}. \quad (95)$$

Why must we call this our “initial form” instead of our final solution? Our issue here is virtually identical to the distinctions we found in Sections 4.1, 4.2, and 4.3 in the treatment of exact rotation matrices vs error-containing measurements of rotation matrices. When we use error-containing data for the pose problem, the perfect match of Eq. (94) and its extension to an actual 3×3 camera model matrix in Eq. (95) breaks down, just as it did when we introduced the data-generic Bar-Itzhack method in Section 4.3. As soon as we insert data with errors in these equations, the different components are *not even normalized to unity*, much less orthogonal. This cannot be the optimal answer for a rotation matrix placing a noisy 2D point image into a corresponding 3D cloud scene. It will still be a least-squares solution minimizing the cost function Eq. (87), but since it does not preserve the properties of a rotation matrix, it will not actually correspond to an optimal *rotation*, which is what we require of the pose estimation problem.

Finally, we can *reverse-engineer* a new version of the adjugate variables in Eq. (93) found by hand-solving the least-squares optimization. We know that Eq. (95) corresponds with the adjugate variables via Eq. (83), so if we simply solve that for the q_{ij} , we find the

adjugate variables in directly in terms of the cross-covariance determinants that produce Eq. (95):

$$\left. \begin{aligned} q_{00} &\rightarrow \frac{1}{4d_1}(d_1 + d_{10} - d_5 + d_7) \\ q_{11} &\rightarrow \frac{1}{4d_1}(d_1 - d_{10} + d_5 + d_7) \\ q_{22} &\rightarrow \frac{1}{4d_1}(d_1 - d_{10} - d_5 - d_7) \\ q_{33} &\rightarrow \frac{1}{4d_1}(d_1 + d_{10} + d_5 - d_7) \\ q_{01} &\rightarrow \frac{1}{4d_1}(d_9 - d_3) \\ q_{02} &\rightarrow \frac{1}{4d_1}(d_2 - d_6) \\ q_{03} &\rightarrow \frac{1}{4d_1}(d_4 + d_8) \\ q_{23} &\rightarrow \frac{1}{4d_1}(d_3 + d_9) \\ q_{13} &\rightarrow \frac{1}{4d_1}(d_2 + d_6) \\ q_{12} &\rightarrow \frac{1}{4d_1}(d_8 - d_4) \end{aligned} \right\} . \quad (96)$$

The Adjugate and the Solution to the 3D Pose Estimation Problem. Let us state our problem clearly: we have a least squares solution that works on all data, but that solution corresponds to a rotation matrix only for perfect data. This latter behavior is almost certainly a manifestation of the rotation-invariant eigenvalues that occur for perfect data in the 3D cloud alignment problem of Section 5.3, outlined in Appendix B. To solve the problem, we must *restrict the subspace of solutions to pure rotations*. But we know *exactly* how to accomplish that! We simply take our “good approximation,” namely our initial solution $\tilde{R}(\mathbf{x}; \mathbf{u})$ given in Eq. (95), consider it as an *error-containing rotation matrix*, and apply the Bar-Itzhack optimization as a *second iteration optimization* to produce a new quaternion adjugate corresponding to the perfect rotation matrix *best approximating* our initial formula Eq. (95); this rotation will then apply in both the case of perfect data and in the more general case when, as we can see, the data themselves produce a completely reasonable example of an inexact rotation matrix that must be optimized. We would argue that no more accurate least-squares-related pure rotation matrix solving the pose estimation problem can be found; without question this solves the perfect-data pose problem, and very plausibly is the best solution to the errorful-data pose estimation problem.

For completeness, we review the actual steps producing a closed form algebraic solution to the 3D Pose task. First, we examine the matrix Eq. (95), which in the errorful-data case effectively is the cross-covariance matrix appearing in the 3D Match task Eq. (80). While the expression \tilde{R} of Eq. (95) is a rotation matrix for perfect data, and continues to give a least squares solution minimizing Eq. (87) for noisy data, it no longer obeys all the constraints needed to make it a valid rotation matrix. We can thus apply the Bar-Itzhack

optimization we explored earlier to find the *nearest* rotation matrix to Eq. (95). Since the Bar-Itzhack loss function needs the *inverse* of the desired approximate matrix to find the quaternion of the closest pure rotation matrix, we now compute the profile matrix of the *transpose* of \tilde{R} , Eq. (95), which, from Eq. (82), now becomes:

$$M(x, y, z; u, v) = \begin{bmatrix} d_7 - d_5 + d_{10} & -(d_9 - d_3) & -(d_2 - d_6) & -(d_8 + d_4) \\ -(d_9 - d_3) & d_7 + d_5 - d_{10} & d_8 - d_4 & d_6 + d_2 \\ -(d_2 - d_6) & d_8 - d_4 & -d_7 - d_5 - d_{10} & d_3 + d_9 \\ -(d_8 + d_4) & d_6 + d_2 & d_3 + d_9 & -d_7 + d_5 + d_{10} \end{bmatrix}, \quad (97)$$

that is, the last three rows of the first column, and the last three columns of the first row are negated to correspond to the matrix \tilde{R}^t . We then compute the maximal eigenvalue using any method we like, but we note that it is not hard to compute the analytic algebraic formula using the Cardano equations (Hanson, 2020). Given that eigenvalue

$$\lambda_{\max} = (\mathbf{Maximal\ Eigenvalue}) (M(x, y, z; u, v)) , \quad (98)$$

we form the characteristic matrix χ with vanishing determinant by subtracting λ_{\max} ,

$$\chi(x, y, z; u, v) = [M(x, y, z; uv) - \lambda_{\max} I_4] . \quad (99)$$

Recall that the critical feature is the maximal eigenvector, whose normalized value is the quaternion giving the optimal solution for the sought-for rotation matrix. As usual, we now just compute the adjugate, which, up to a normalization, will now always be four copies of the needed optimal quaternion,

$$A(x, y, z; u, v) = \text{Adjugate}(\chi(x, y, z; u, v)) = \begin{bmatrix} q_0^2 & q_0 q_1 & q_0 q_2 & q_0 q_3 \\ q_0 q_1 & q_1^2 & q_1 q_2 & q_1 q_3 \\ q_0 q_2 & q_1 q_2 & q_2^2 & q_2 q_3 \\ q_0 q_3 & q_1 q_3 & q_2 q_3 & q_3^2 \end{bmatrix} . \quad (100)$$

The final answer is found by choosing a nonsingular row from the adjugate $A(x, y, z; u, v)$ for normalization to determine q_{opt} :

$$q_{\text{opt}} = (\mathbf{Normalize\ Row\ with\ Largest\ Diagonal}) (A(x, y, z; u, v)) . \quad (101)$$

We noted in previous simpler examples that, while q_{opt} can be very complicated, reassembling the quaternions into the rotation matrix itself, $R_{\text{opt}} = R(q_{\text{opt}})$, can result in a simplified final form; we have not yet accomplished that explicitly for the 3D problem, but a differentiable final form of the optimal quaternion can be obtained using the noted algebraic form of the solution.

Note: One finds experimentally an odd feature of this optimization process: because our fundamental standard for optimization is the Fröbenius norm of the 3×3 rotation

matrix differences, the appropriate test of differences is based on the *rotation matrices*. If one compares the *quaternions* resulting from Eq. (101) using a *quaternion distance measure*, one occasionally finds quaternions that are nearly inverses of one another, and thus very far apart. However, examining the resulting rotation matrices, which will also be close to inverses of the expected matrix, one finds that, indeed, the inverse-like rotation matrix will correspond to a *smaller* Fröbenius norm, and so is technically correct. This phenomenon, which seems to appear for $|q_0| \ll 1$, is one of many odd features appearing when we add substantial noise to rotation matrices.

To bring this to a close, we test our new solutions using randomly generated 3D point clouds and corresponding 2D projections after a rotation and added noise (Fig. (5)). For each data set, we consider both the exact solution Eq. (95), which gives a valid rotation matrix only for noise-free data but always minimizes the least-squares, as well as the solution after applying Bar-Itzhack via the profile matrix Eq. (97). When we compute these and compare the list of losses to those of the original rotation used to simulate the pose data, we find we outperform this original rotation matrix (referred to as *rot_mat*) and our results improve as more noise is added (Fig. (5)). The least squares solution, which is not a rotation for noisy data, can be even better, but of course those results are not useful. We also checked these results for zero noise, and our optimal rotation and the original rotation substituted into the loss function are uniformly zero to machine accuracy $\approx 10^{-30}$, consistent with an exact least-squares loss minimizing solution to the pose estimation optimization problem.

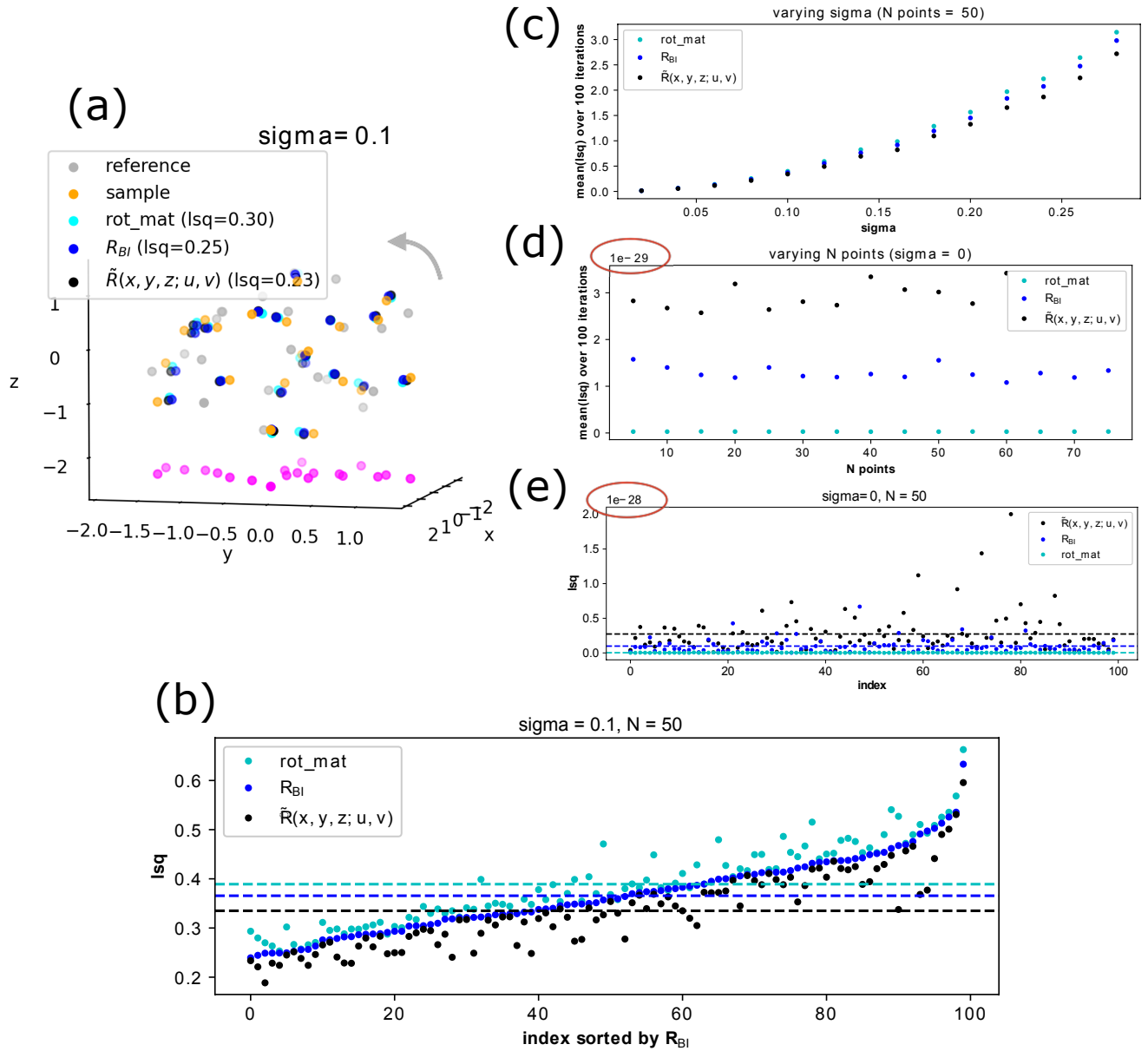


Figure 5: **Results using Analytical Solution to the 3D Point-Cloud Projection Problem.** (a) Example data for a small rotation with noise $\sigma = 0.1$: original reference data in grey, rotated sample points in orange, points using rotation matrix without noise in cyan, our analytical solution $\tilde{R}(x, y, z; u, v)$ in blue, the rotation-corrected solution R_{BI} in black, and projected points in magenta. (b) Comparison of least squared errors between our analytical solution $\tilde{R}(x, y, z; u, v)$ in blue, the rotation-corrected solution R_{BI} in black, and the original rot_mat in cyan for 100 random 3D point clouds with $N = 50$ and $\sigma = 0.1$. Data are sorted by the R_{BI} results, and dashed lines indicate the mean. (c) Exploration of the dependency of the least squared errors on σ , here with $N = 50$, and we plot the mean results over 100 iterations. The coloring is as in (b). (d,e) Exploring the no-noise case for $\tilde{R}(x, y, z; u, v)$ and R_{BI} : the original rot_mat performs consistently better, but without any dependency on the number of points; one set of 100 iterations with $N = 50$ is shown for clarity. In both cases note that the scale of the y axis is 10^{-29} .

5.5 3D Pose Estimation with Perspective Projection

We have assumed that orthographic projection could be used in our 2D and 3D Pose estimation exercises so far in order to find closed-form least squares solutions for optimal adjugate matrices of unnormalized quaternions and their corresponding rotation matrices. Pieces of our solution methods can be applied also to the more difficult problem of perspective projection, with finite focal length. For our final application, we now explore an approach to perspective 3D pose estimation that exploits the same methods as the previous parts of this Section.

We will make no attempt to review the vast literature on this subject, but it is appropriate to mention a few of the influential developments along with more current pieces of literature, starting with the classic work of Haralick et al. Haralick et al. (1989), which defines the problem for the case of corresponding points, which has been our context throughout. Weintapper et al. and Zhou et al. Wientapper and Kuijper (2016); Wientapper et al. (2018); Zhou et al. (2020) continue with some recent developments of the classic methods. Lu et al. (2000) invoke an approach similar to ours, utilizing multiple stages, but without the closed-form aspects that we are available to us, Guo et al. (2021) study other approaches, while related quaternion methods are employed by Barfoot et al. (2011). We focus exclusively on the rotation aspects, but a number of authors examine full 6 degree-of-freedom methods, most recently making heavy use of machine learning, such as, e.g., Xiang et al. (2018); Hu et al. (2020).

We start as usual with a loss function based on least squares that needs to be minimized in order to find the rotation matrix that rotates a 3D reference cloud to its best possible alignment with a planar 2D image. While we were able to get away with just the top two lines of the rotation matrix in the orthographic projection squared-error function, now we need the entire matrix because the bottom row determines the depth coordinate that implements the perspective division. Thus we start with the two-row projection Eq. (88) determining the numerator of the rotated 3D cloud, and adjoin to that the 3rd line in quaternion adjugate coordinates

$$R_3 = D(q) = \begin{bmatrix} 2q_{13} - 2q_{02} & 2q_{23} + 2q_{01} & q_{00} - q_{11} - q_{22} + q_{33} \end{bmatrix}$$

to produce the relevant depth element $z' = D(q) \cdot [x, y, z]$.

Alternate Choices of Camera Location. We can choose from two alternative ways of looking at the least squares loss function for perspective projection, illustrated in Fig. (6) and Fig. (7) noting that a perspective projection loss function analogous to the orthographic loss Eq. (87) must incorporate an additional division by the depth. One traditional approach places the point cloud's center of mass at the origin and the image plane at $z = 0$, with the camera looking down from a pinhole camera at focal distance f , so $x_{\text{cam}} = (0, 0, f)$. This has the advantage that the similar-triangles perspective formula contains only the inverse

focal length $\bar{f} = 1/(\text{focal length})$ multiplying the depth:

$$\mathbf{S}_{\text{3D Pose } \bar{f}} = \mathbf{S}(\bar{f}) = \sum_{k=1}^K \left\| \frac{P(q) \cdot \mathbf{x}_k}{(1 - \bar{f} D(q) \cdot \mathbf{x}_k)} - \mathbf{u}_k \right\|^2. \quad (102)$$

This form allows one to easily take the orthographic limit $\bar{f} \rightarrow 0$ without needing infinite numbers. An alternative perspective formula commonly used in machine vision reverses the camera and the point cloud, so the camera is at the origin, the image is at $z = f$, and the cloud center of mass is off-center at $(0, 0, f)$, so the similar-triangles computation yields the least squares expression involving only f , as opposed to only $\bar{f} = 1/f$:

$$\mathbf{S}_{\text{3D Pose } f} = \mathbf{S}(f) = \sum_{k=1}^K \left\| \frac{f P(q) \cdot \mathbf{x}_k}{D(q) \cdot \mathbf{x}_k} - \mathbf{u}_k \right\|^2. \quad (103)$$

The cloud-driven geometry of these two approaches is shown in Fig. (6) and Fig. (7). In either case, we will assume that the focal point of the pinhole camera appears well outside the cloud so that the optimization problem has smooth mathematical behavior.

Remark on focal length determination. The focal length can be determined from the data at any stage by setting the derivative of $\mathbf{S}(f)$ or $\mathbf{S}(\bar{f})$ to zero and solving for f or \bar{f} , provided one has a candidate for the rotation matrix $R(q_{\text{opt}}) = [P(q_{\text{opt}}), D(q_{\text{opt}})]$. However, the \bar{f} version results upon differentiation in a very high degree formula in \bar{f} whose vanishing point needs to be found numerically, though it is typically well-behaved. In contrast, given some known $R(q_{\text{opt}})$ that produces $R(q_{\text{opt}}) \cdot [x, y, z] = [x', y', z']$, the f version gives a closed form solution that is simply

$$f = \frac{\sum_{k=1}^K ((u_k x'_k + v_k y'_k)/z'_k)}{\sum_{k=1}^K ((x'_k{}^2 + y'_k{}^2)/z'_k{}^2)}. \quad (104)$$

While we propose an iterative three-step solution in Appendix E, here we simply test our orthographic solutions \tilde{R} and R_{BI} , described above by Eq. (95), and Eq. (97), against existing solutions for the perspective pose estimation problem, with the difference that the least-squares loss is measured as described in Eq. (102) or Eq. (103), appropriately. In Fig. (6) we study the case in which the point cloud is at the origin, and compare to the iterative LHM method (Lu et al., 2000). In Fig. (7), we have adapted the available MatLab code for the MLPnP method as in (Urban et al., 2016) to study the case where the camera is at the origin, and compare our orthographic results to both LHM and MLPnP. In all cases, we employ noisy ($\sigma = 0.1$) data, comparing different focal lengths, and in the case of the MLPnP tests, different numbers of points N . For the MLPnP tests, we supplement our least-squares measure with a quaternion-quaternion distance measure, to be more similar to the existing literature (e.g., Urban et al. (2016)). Here we use the quaternion-quaternion angle measure,

$$\text{Rotation Error}(q_{\text{opt}}, q_0) = 2 \arccos(q_{\text{opt}} \cdot q_0), \quad (105)$$

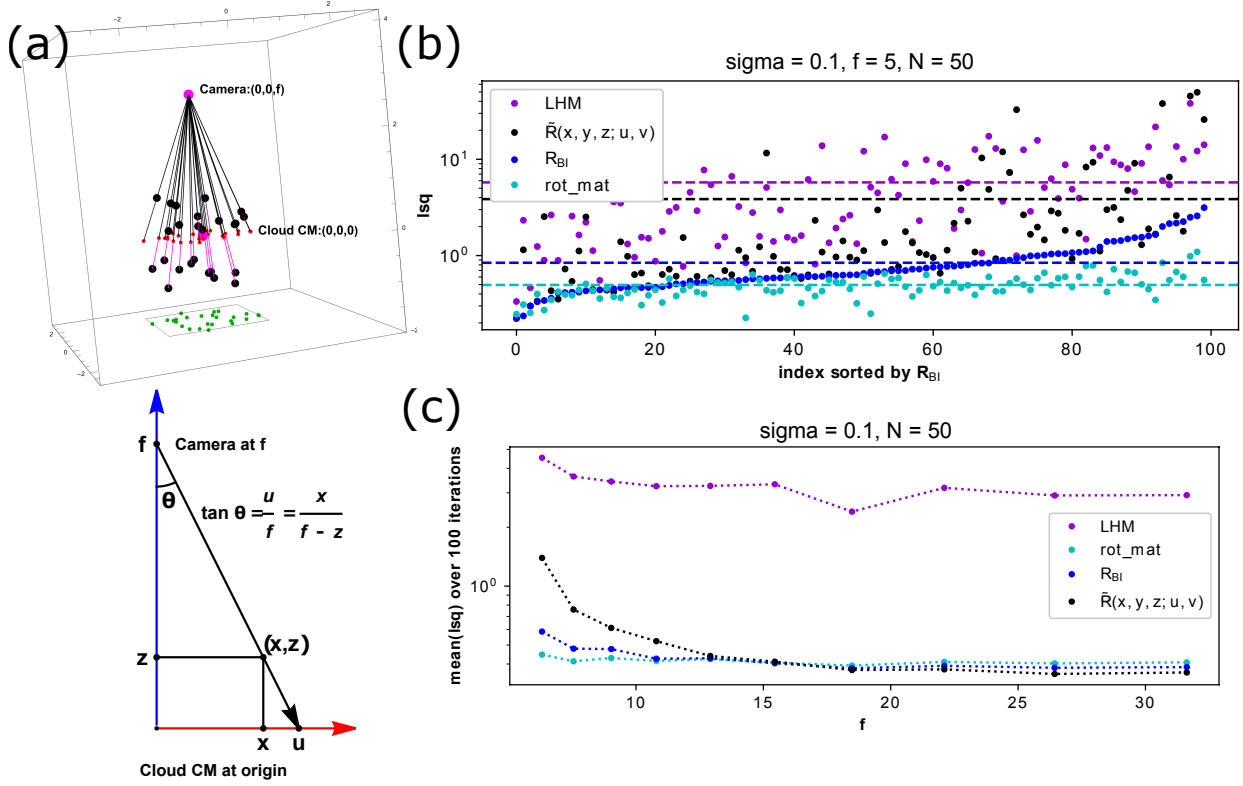


Figure 6: **3D Perspective Pose Problem and Loss Spectra: Camera at $z = f$.** (a) Geometry of perspective projection from camera at $(0, 0, f)$ from the 3D reference data to centered at the origin noisy 2D image, with $u/f = x/(f - z)$ defining the projected coordinates (u, v) . (b) Plotting the values of the 3D perspective loss function of Eq. (102) with focal length f for the 3D Pose estimation problem, comparing the original data-generating rotation rot_mat , the LHM method’s results (Lu et al., 2000), our closed-form least squares solution \tilde{R} , and the corrected exact rotation R_{BI} . An error distribution with $\sigma = 0.1$ is used for the simulated projection data with 50 points. (c) The mean least-squares error averaged over 100 sample data sets of size 50 with normal error $\sigma = 0.1$ as a function of the focal length f , on a logarithmic scale. The R_{BI} rotation solution does very well at smaller focal lengths, while \tilde{R} (not a rotation) least-squares solution gets better at large camera distances, and R_{BI} appears to outperform the LHM.

where q_0 is chosen to be the RMSD solution between the reference 3D point cloud and the sample 3D point cloud after rotation and added noise, but before projection.

It is plain to see that in both Fig. (6) and Fig. (7), our R_{BI} rotation matrix outperforms both LHM and MLPnP, with improved performance at longer focal lengths, as would be expected given our orthographic assumption.

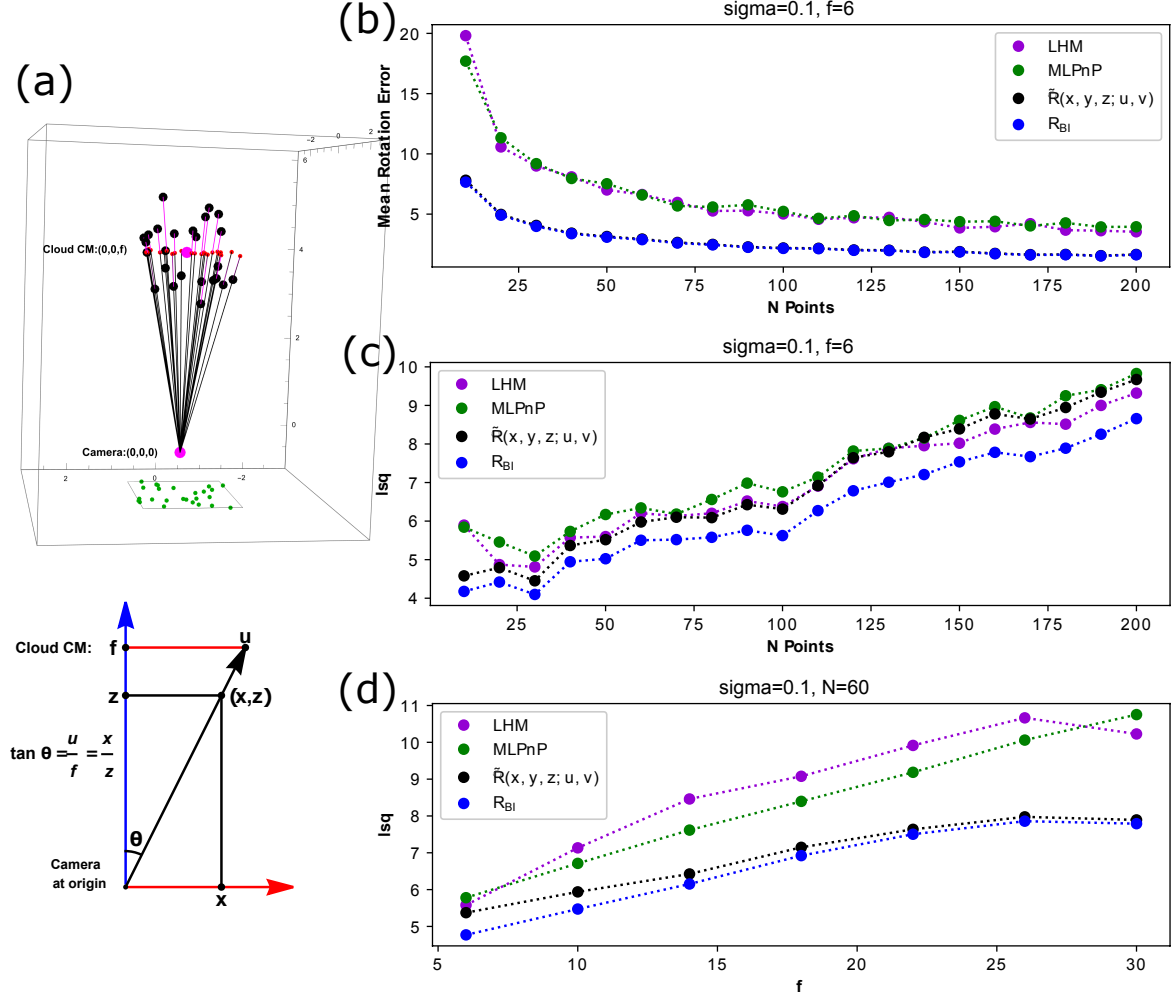


Figure 7: **3D Perspective Pose Problem and Loss Spectra: Camera at Origin.** (a) Geometry of perspective projection from camera at $(0,0,0)$ to 3D reference data centered at $(0,0,f)$, producing a noisy 2D image, with $u/f = x/f$ defining the projected coordinates (u,v) . (b) For 3D point cloud sizes ranging from 10 to 200, random quaternion rotations were applied to produce noisy 2D projected images with standard error $\sigma = 0.1$ and focal length 6. We plot the relative performances of the LHM and MLPnP algorithms compared to ours using our version of the “Mean (Quaternion) Rotation Error” in Eq. (105). In this context, our idealized least-squares solution \hat{R} and our corrected-to-robust-rotation solution R_{BI} are basically indistinguishable, with \hat{R} ’s black dots hidden behind the blue dots of R_{BI} . (c) For the same collection of point-cloud sizes and parameters, we plot the corresponding 3D pose least-squares measure Eq. (103), and find similar results, with the optimal-rotation solution R_{BI} responding best to this measure. (d) Here we fix the cloud sample size at 60 and plot mean least-squares measure across a spectrum of different focal lengths. Again, R_{BI} shows a good response.

5.6 Remarks

Properties of variational approaches: The algebraic solution methods we have outlined here are not necessarily the most effective approach. In particular, numerical approximation methods involving *argmin* or *argmax* numerical searches for the numerical optimization of the loss functions that we have considered here can be quite effective, and can efficiently enforce constraints on either the quaternion variables themselves, or on the adjugate variables. The latter have the advantage of course that the singular domains of the quaternion determination can be explicitly avoided, and the constraints essentially function as Lagrange multipliers if the optimization is considered as a dynamical system. Similarly, trainable neural networks can function more or less equivalently to numerical search optimization, with the particular advantage that, if successfully trained, the expensive search process in an *argmin* implementation, which is repeated for each and every new data instance, is skipped in every later application of a neural network. Using the loss functions that we have presented to implicitly guide the training target *without explicit training data* is basically the same context as *argmin*, except that the resulting successful search path can be efficiently encoded for arbitrary future exploitation using one-time trained weights. Strategies parallel to the *argmin* method using the adjugate variable approach to the loss function can clearly be implemented using neural networks, and such approaches should be effective for pose estimation. Constraints can supplement the loss function used to update the weights (to function much the same as Lagrange multipliers) in a neural network’s virtual dynamical system. We intend to treat these issues in detail elsewhere.

Possible applications to multiple datasets, bundle adjustment, and cryo-EM:

Here we have studied optimal alignment of single datasets with a single rigid point cloud and a single camera model. Many important applications examine collections of camera models providing an assembly of data imposing restrictions on one or more imprecisely known point clouds. For example, the bundle adjustment problem (Schönberger and Frahm, 2016; Schönberger et al., 2016; Triggs et al., 2000; Chen et al., 2016; Remondino et al., 2017) examines a collection of camera models, optimizes them individually, and then optimizes them collectively in combination with the optimization of the candidate point cloud coordinates. This problem has many properties in parallel with the field of cryo-EM single particle analysis (see, e.g. Scheres, 2012; Punjani et al., 2017; Zivanov et al., 2018; Singer and Sigworth, 2020) which determines the 3D structure of a molecule from a collection of 2D images of that molecule. The techniques that we have introduced here may also be able to contribute to the multiple dataset problem.

6 Conclusion

Our objective in this paper has been to establish a clear framework for understanding how quaternions must be treated in the context of measurable rotation matrices, whatever the source. There are many domains in which the use of quaternions for representing rotations is attractive, and some recent papers (Zhou et al., 2019; Peretroukhin et al., 2020; Zhao et al., 2020; Xiang and Li, 2020) have cast doubt on the validity of quaternions as an output parameterization for automatic learning of the quaternion corresponding to implicit or explicit rotation matrices. We have shown that a variational method based on the work of Bar-Itzhack (2000) recasts both ideal and noisy rotation measurements into the framework of an adjugate matrix; this matrix contains four separate algebraic formulas for the same quaternion corresponding to a given rotation matrix. Each expression is valid in a certain region of the quaternion manifold \mathbf{S}^3 , but breaks down with a singularity in the normalization outside its own region. Combined, however, these four formulas, actually eight if we include their opposite signs, completely cover the quaternion manifold with nonsingular patches. The natural occurrence of these singular regions and the ways to escape them by crossing between formulas to cover the whole manifold then allow us to understand quaternions from a consistent mathematical viewpoint.

Having established the importance of the adjugate, we adopted the quaternion adjugate variables, substituting single adjugate variables for all possible quadratic quaternion forms, as a framework for treating matching and pose estimation problems. This is of interest because algebraic problems using quaternion variables are reduced in degree by a factor of two in the adjugate variables. The cost of this transformation is the introduction of additional constraints, but in certain cases the advantage of using the adjugate variables instead of bare quaternions can be significant. Using this framework, we were able to solve the pose estimation problem with orthographic projection, resulting, resulting in closed form least squares solutions valid for perfect data, and correctable to optimal rotations for noisy data using a second-stage Bar-Itzhack optimization. Furthermore, we applied this result successfully to the pose estimation problem with perspective projection, and found that even with the imperfect orthographic approximation our results outperformed those of existing methods. Thus we argue that the adjugate variables not only solve the question of how to understand the quaternion manifold in rotation-determination tasks, but have applications of their own in simplifying certain least squares problems for optimal rotations.

Acknowledgments

We are indebted to B.K.P. Horn for his crucial role in introducing us to this problem, and for continuing support and encouragement, and to Pascal Fua and Yinlin Hu for their generous advice and assistance. SMH acknowledges the support of the Flatiron Institute and many helpful interactions with her colleagues there.

References

- Itzhack Y. Bar-Itzhack. New method for extracting the quaternion from a rotation matrix. *Journal of Guidance, Control, and Dynamics*, 23(6):1085–1087, 2000. doi: doi.org/10.2514/2.4654. URL <https://arc.aiaa.org/doi/abs/10.2514/2.4654>.
- Timothy Barfoot, James R. Forbes, and Paul T. Furgale. Pose estimation using linearized rotations and quaternion algebra. *Acta Astronautica*, 68(1):101–112, 2011. ISSN 0094-5765. doi: <https://doi.org/10.1016/j.actaastro.2010.06.049>. URL <https://www.sciencedirect.com/science/article/pii/S0094576510002407>.
- Yu Chen, Yisong Chen, and Guoping Wan. Bundle adjustment revisited, June 2016. URL <https://arxiv.org/pdf/1912.03858.pdf>.
- Olivier Faugeras and Martial Hebert. A 3D recognition and positioning algorithm using geometrical constraints between primitive surfaces. In *Proc. 8th Joint Conf. on Artificial Intell.*, IJCAI’83, pages 996–1002. Morgan Kaufmann, August 1983. URL <http://dl.acm.org/citation.cfm?id=1623516.1623603>.
- Olivier Faugeras and Martial Hebert. The representation, recognition, and locating of 3D objects. *International Journal of Robotic Research (IJRR)*, 5:27–52, 09 1986. doi: 10.1177/027836498600500302.
- G.H. Golub and C.F. van Loan. *Matrix Computations*. Johns Hopkins University Press, Baltimore, MD, 1st edition, 1983. Sec 12.4.
- K. Guo, H. Ye, Z. Zhao, and J. Gu. An efficient closed form solution to the absolute orientation problem for camera with unknown focal length. *Sensors*, 21:6480, 2021. doi: doi.org/10.3390/s21196480. URL <https://www.mdpi.com/1424-8220/21/19/6480/pdf>.
- Andrew J. Hanson. *Visualizing Quaternions*. Morgan-Kaufmann/Elsevier, 2006.
- Andrew J. Hanson. The quaternion-based spatial-coordinate and orientation-frame alignment problems. *Acta Crystallographica Section A*, 76(4):432–457, Jul 2020. doi: 10.1107/S2053273320002648.
- Robert M. Haralick, Hyonam Joo, Chung-Nan Lee, , Xinhua Zhuang, Vinay G. Vaidya, and Man Bae Kim. Pose estimation from corresponding point data. *IEEE Transactions on Systems, Man, and Cybernetics*, 19(6):1426–1446, November/December 1989. URL https://haralick.org/journals/Pose_estimation_from_corresponding_points.pdf.

- B. K. P. Horn. Closed-form solution of absolute orientation using unit quaternions. *J. Opt. Soc. Am. A*, 4:629–642, April 1987. URL <https://www.osapublishing.org/josaa/viewmedia.cfm?uri=josaa-4-4-629&seq=0>.
- Yinlin Hu, Pascal Fua, Wei Wang, and Mathieu Salzmann. Single-stage 6D object pose estimation. *Conference on Computer Vision and Pattern Recognition (CVPR)*, pages 2927–2936, June 2020. ISSN 1063-6919. doi: 10.1109/CVPR42600.2020.00300. URL <https://infoscience.epfl.ch/record/276422>.
- Chien-Ping Lu, Gregory D. Hager, and Eric Mjolsnes. Fast and globally convergent pose estimation from video images. *IEEE Transactions on Pattern Analysis and Machine Intelligence*, 22(6), June 2000.
- C. Olsson, F. Kahl, and M. Oskarsson. The registration problem revisited: Optimal solutions from points, lines and planes. In *International Conference on Computer Vision and Pattern Recognition (CVPR)*, pages 1206–1213, 2006.
- Valentin Peretroukhin, Matthew Giamou, W. Nicholas Greene, David Rosen, Jonathan Kelly, and Nicholas Roy. A smooth representation of belief over $SO(3)$ for deep rotation learning with uncertainty. *Robotics: Science and Systems XVI*, Jul 2020. doi: 10.15607/rss.2020.xvi.007. URL <http://dx.doi.org/10.15607/RSS.2020.XVI.007>.
- Ali Punjani, John L Rubinstein, David J Fleet, and Marcus A Brubaker. cryosparc: algorithms for rapid unsupervised cryo-em structure determination. *Nature Methods*, 14:290–296, 2017.
- Fabio Remondino, Erica Nocerino, Isabella Toschi, and Fabio Menna. A critical review of automated photogrammetric processing of large datasets, 2017.
- Soheil Sarabandi and Federico Thomas. Accurate computation of quaternions from rotation matrices. In J. Lenarcic and V. Parenti-Castelli, editors, *Advances in Robot Kinematics 2018. ARK 2018*, volume 8 of *Springer Proceedings in Advanced Robotics*, pages 1–8. Springer, Cham., 2019. doi: https://doi.org/10.1007/978-3-319-93188-3_5.
- Soheil Sarabandi, Alba Perez-Gracia, and Federico Thomas. Singularity-free computation of quaternions from rotation matrices in \mathbb{E}^4 and \mathbb{E}^3 . In *Conference on Applied Geometric Algebras in Computer Science and Engineering*, pages 23–27, July 2018.
- Soheil Sarabandi, Arya Shabani, Josep M. Porta, and Federico Thomas. On closed-form formulas for the 3D nearest rotation matrix problem. *IEEE Transactions on Robotics*, 36(4):1333–1339, 2020. URL <https://www.iri.upc.edu/people/thomas/papers/IEEE%20TRO%202020.pdf>.
- A. Saxena, J. Driemeyer, and A. Y. Ng. Learning 3D object orientation from images. In *IEEE Inter. Conf. Robotics and Automation (ICRA '09)*, pages 794–800, 2009.
- Sjors H.W. Scheres. Relion: Implementation of a bayesian approach to cryo-em structure determination. *Journal of Structural Biology*, 180(3):519–530, 2012. ISSN 1047-8477. doi: <https://doi.org/10.1016/j.jsb.2012.09.006>. URL <https://www.sciencedirect.com/science/article/pii/S1047847712002481>.

- Johannes Lutz Schönberger and Jan-Michael Frahm. Structure-from-motion revisited. In *Conference on Computer Vision and Pattern Recognition (CVPR)*, 2016.
- Johannes Lutz Schönberger, Enliang Zheng, Marc Pollefeys, and Jan-Michael Frahm. Pixelwise view selection for unstructured multi-view stereo. In *European Conference on Computer Vision (ECCV)*, 2016.
- S. W. Shepperd. Quaternion from rotation matrix. *Journal of Guidance and Control*, 1(3):223–224, 1978.
- Amit Singer and Fred J. Sigworth. Computational methods for single-particle cryo-em, 2020. URL <https://arxiv.org/abs/2003.13828>.
- Bill Triggs, Philip F. McLauchlan, Richard I. Hartley, and Andrew W. Fitzgibbon. Bundle adjustment : A modern synthesis. In B. Triggs, A. Zisserman, and R. Szeliski, editors, *Vision Algorithms '99, LNCS 1883*, pages 298–372. Springer-Verlag, Berlin, Heidelberg, 2000.
- S. Urban, J. Leitloff, and S. Hinz. MLPnP - a real-time maximum likelihood solution to the perspective-n-point problem. *ArXiv*, abs/1607.08112, June 2016. doi: 0.5194/isprsannals-III-3-131-2016.
- F. Wientapper and A. Kuijper. Unifying algebraic solvers for scaled Euclidean registration from point, line and plane constraints. In *Asian Conference on Computer Vision*, pages 52–66. Springer, 2016.
- F. Wientapper, M. Schmitt, M. Fraissinet-Tachet, and A. Kuijper. A universal closed-form approach for absolute pose problems. *Computer Vision and Image Understanding*, 173:57–77, 2018. URL <https://www.sciencedirect.com/science/article/pii/S1077314218300572>.
- Sitao Xiang and Hao Li. Revisiting the continuity of rotation representations in neural networks, 2020. URL <https://arxiv.org/abs/2006.06234>.
- Yu Xiang, Tanner Schmidt, Venkatraman Narayanan, and Dieter Fox. Posecnn: A convolutional neural network for 6d object pose estimation in cluttered scenes. In *Robotics: Science and Systems 2018*, pages 1–10, 06 2018. doi: 10.15607/RSS.2018.XIV.019.
- Yongheng Zhao, Tolga Birdal, Jan Eric Lenssen, Emanuele Menegatti, Leonidas Guibas, and Federico Tombari. QEC: Quaternion equivariant capsule networks for 3d point clouds, 2020. URL <https://arxiv.org/abs/1912.12098>.
- Lipu Zhou, Shengze Wang, and Michael Kaess. A fast and accurate solution for pose estimation from 3d correspondences. In *2020 IEEE International Conference on Robotics and Automation (ICRA)*, pages 1308–1314, 05 2020. doi: 10.1109/ICRA40945.2020.9197023. URL <https://www.cs.cmu.edu/~kaess/pub/Zhou20icra.pdf>.
- Yi Zhou, Connelly Barnes, Jingwan Lu, Jimei Yang, and Hao Li. On the continuity of rotation representations in neural networks. In *Proceedings of the IEEE/CVF Conference on Computer Vision and Pattern Recognition (CVPR)*, pages 5745–5753, June 2019.

Jasenko Zivanov, Takanori Nakane, Bjorn Forsberg, Dari Kimanius, Wim JH Hagen, Erik Lindahl, and Sjors HW Scheres. New tools for automated high-resolution cryo-em structure determination in relion-3. *eLife*, 7:e42166, nov 2018. ISSN 2050-084X. doi: 10.7554/eLife.42166. URL <https://doi.org/10.7554/eLife.42166>.

A Example Code for Rotation to Quaternion Algorithm

A.1 Pseudocode

Compute the trace of R : $\text{tr} = \text{Trace}(R)$, noting that $\text{tr} = 1 + 2 \cos \theta$.

(if) *if* $\text{tr} > 0$, then set $q_0 = \frac{\sqrt{\text{tr}+1}}{2} = \cos(\theta/2)$.

Compute $s = (2\sqrt{\text{tr}+1})^{-1} = (4 \cos(\theta/2))^{-1}$, then

set $q_1 = s * (m_{32} - m_{23})$, $q_2 = s * (m_{13} - m_{31})$, $q_3 = s * (m_{21} - m_{12})$

(else) *else* check m_{ii} :

if m_{11} is largest, set $s = \sqrt{m_{11} - m_{22} - m_{33} + 1}$

set $q_1 = s/2$, set $s = 1/(2s)$

set $q_0 = s * (m_{3,2} - m_{2,3})$, $q_2 = s * (m_{2,1} - m_{1,2})$, $q_3 = s * (m_{1,3} - m_{3,1})$

if m_{22} is largest, set $s = \sqrt{m_{22} - m_{33} - m_{11} + 1}$

set $q_2 = s/2$, set $s = 1/(2s)$

set $q_0 = s * (m_{1,3} - m_{3,1})$, $q_3 = s * (m_{3,2} - m_{2,3})$, $q_1 = s * (m_{2,1} - m_{1,2})$

if m_{33} is largest, set $s = \sqrt{m_{33} - m_{11} - m_{22} + 1}$

set $q_3 = s/2$, set $s = 1/(2s)$

set $q_0 = s * (m_{2,1} - m_{1,2})$, $q_1 = s * (m_{1,3} - m_{3,1})$, $q_2 = s * (m_{3,2} - m_{2,3})$

Normalize to unity.

A.2 C code

```
typedef struct tag_Quat {double w, x, y, z;} Quat;

/* quat->w is the scalar component, translated here
   internally as q[3] to facilitate the manipulation of
   the vector, or imaginary component, using indices 0,1,2 */

MatToQuat(double m[4][4], Quat * quat)
{ double tr, s, q[4]; int i, j, k; int nxt[3] = {1, 2, 0};

  tr = m[0][0] + m[1][1] + m[2][2];

  /* check the diagonal */
  if (tr > 0.0) {
    s = sqrt (tr + 1.0);
    quat->w = s / 2.0;
    s = 0.5 / s;
    quat->x = (m[2][1] - m[1][2]) * s;
    quat->y = (m[0][2] - m[2][0]) * s;
    quat->z = (m[1][0] - m[0][1]) * s;
  } else {
    /* diagonal is negative */
    i = 0;
    if (m[1][1] > m[0][0]) i = 1;
    if (m[2][2] > m[i][i]) i = 2;
    j = nxt[i];
    k = nxt[j];

    s = sqrt ((m[i][i] - (m[j][j] + m[k][k])) + 1.0);

    q[i] = s * 0.5;

    if (s != 0.0) s = 0.5 / s;

    q[3] = (m[k][j] - m[j][k]) * s;
    q[j] = (m[i][j] + m[j][i]) * s;
    q[k] = (m[i][k] + m[k][i]) * s;

    quat->x = q[0];
    quat->y = q[1];
    quat->z = q[2];
    quat->w = q[3];
  }
}
```

A.3 Mathematica Code

```
(* This code randomizes the sign of q0 in the final step. This is optional. *)

RotToQuat[mat] := Module[{qinit, q0, q1, q2, q3, trace, s, t1, t2, t3},
  trace = Sum [mat[[i, i]], {i,1,3}];
  If[trace > 0,
    s = Sqrt[trace + 1];
    q0 = s/2; s = 1/(2 s);
    q1 = (mat[[3, 2]] - mat[[2, 3]]) s;
    q2 = (mat[[1, 3]] - mat[[3, 1]]) s;
    q3 = (mat[[2, 1]] - mat[[1, 2]]) s,
    If[mat[[1, 1]] ≥ mat[[2, 2]] && mat[[1, 1]] ≥ mat[[3, 3]],
      s = Sqrt[mat[[1, 1]] - mat[[2, 2]] - mat[[3, 3]] + 1];
      q1 = s/2;
      s = 1/(2 s);
      q0 = (mat[[3, 2]] - mat[[2, 3]]) s;
      q2 = (mat[[2, 1]] + mat[[1, 2]]) s;
      q3 = (mat[[1, 3]] + mat[[3, 1]]) s,
      If[mat[[1, 1]] < mat[[2, 2]] && mat[[1, 1]] ≥ mat[[3, 3]],
        s = Sqrt[mat[[2, 2]] - mat[[3, 3]] - mat[[1, 1]] + 1];
        q2 = s/2; s = 1/(2 s);
        q0 = (mat[[1, 3]] - mat[[3, 1]]) s;
        q3 = (mat[[3, 2]] + mat[[2, 3]]) s;
        q1 = (mat[[2, 1]] + mat[[1, 2]]) s,
        s = Sqrt[mat[[3, 3]] - mat[[1, 1]] - mat[[2, 2]] + 1];
        q3 = s/2; s = 1/(2 s);
        q0 = (mat[[2, 1]] - mat[[1, 2]]) s;
        q1 = (mat[[1, 3]] + mat[[3, 1]]) s;
        q2 = (mat[[3, 2]] + mat[[2, 3]]) s];];
  qinit = N[{q0, q1, q2, q3}];
  qinit = If[Abs[q0] < 10-10, qinit, Sign[q0] qinit];
  qinit = (1 - 2 RandomInteger[{0, 1}]) qinit;
  Normalize[qinit]]
```

B Invariance of the Matching Problem Eigenvalues for Error-Free Data

In most realistic cases of the 3D Match problem, attempting to find the best rotation to align a cloud that is misoriented with respect to a the reference cloud of its origin, the sample data occur multiple times, with each instance related to the reference data by a rotation, *and* the sample data are somewhat noisy, so that they do not correspond exactly to a pure rotation applied to the reference data. However, a particularly interesting feature appears if there is no noise, or if the noise is effectively negligible. In this case, the self-covariance of the reference data completely determines the eigenvalue of the profile matrix for each sample, and, since the loss function for each sample is exactly the eigenvalue, they cannot be distinguished. The *eigenvectors* corresponding to that one single eigenvalue are of course distinct, and, treated as quaternions, they determine which rotation must be applied to align each distinct sample with the reference data.

This feature of the "ideal" noise-free situation can be proven as follows: first we take a reference data set of K 3D points $Y = \{y_k\}$ and a given pairwise-matched sample data set $X = \{x_k\}$, with each such point having a 3D index $a \in \{1, 2, 3\}$, e.g., $[x_k]_a$. Then we deal with the cross-covariance matrix,

$$E_{ab} = \sum_{k=1}^N [x_k]_a [y_k]_b = [\mathbf{X} \cdot \mathbf{Y}^t]_{ab} \quad (106)$$

where $[x_k]$ denotes the k th column of \mathbf{X} , and the range of the indices (a, b) is the spatial dimension $D = 3$, and we examine the cross-term of the least-squares loss for the matching problem

$$\Delta(q) = \text{tr } R(q) \cdot E = (q_0, q_1, q_2, q_3) \cdot M(E) \cdot (q_0, q_1, q_2, q_3)^t \equiv q \cdot M(E) \cdot q. \quad (107)$$

Here $M(E)$ is the traceless, symmetric 4×4 matrix

$$M(E) = \begin{bmatrix} E_{xx} + E_{yy} + E_{zz} & E_{yz} - E_{zy} & E_{zx} - E_{xz} & E_{xy} - E_{yx} \\ E_{yz} - E_{zy} & E_{xx} - E_{yy} - E_{zz} & E_{xy} + E_{yx} & E_{zx} + E_{xz} \\ E_{zx} - E_{xz} & E_{xy} + E_{yx} & -E_{xx} + E_{yy} - E_{zz} & E_{yz} + E_{zy} \\ E_{xy} - E_{yx} & E_{zx} + E_{xz} & E_{yz} + E_{zy} & -E_{xx} - E_{yy} + E_{zz} \end{bmatrix}. \quad (108)$$

built from our original 3×3 cross-covariance matrix E defined by Eq. (106). We will refer to $M(E)$ from here on as the *profile matrix*.

We begin by writing down the eigenvalue expansion of the profile matrix,

$$\det[M - eI_4] = e^4 + e^3 p_1 + e^2 p_2 + e p_3 + p_4 = 0, \quad (109)$$

where e denotes a generic eigenvalue, I_4 is the 4D identity matrix, and the p_k are homogeneous polynomials of degree k in the elements of M . For the special case of a traceless, symmetric profile matrix $M(E)$ defined by Eq. (108), the $p_k(E)$ coefficients simplify and can be expressed numerically as the following functions either of M or of E :

$$p_1(E) = -\text{tr}[M] = 0 \quad (110)$$

$$\begin{aligned} p_2(E) &= -\frac{1}{2} \text{tr}[M \cdot M] = -2 \text{tr}[E \cdot E^t] \\ &= -2 (E_{xx}^2 + E_{xy}^2 + E_{xz}^2 + E_{yx}^2 + E_{yy}^2 + E_{yz}^2 + E_{zx}^2 + E_{zy}^2 + E_{zz}^2) \end{aligned} \quad (111)$$

$$\begin{aligned} p_3(E) &= -\frac{1}{3} \text{tr}[M \cdot M \cdot M] = -8 \det[E] \\ &= 8 (E_{xx} E_{yz} E_{zy} + E_{yy} E_{xz} E_{zx} + E_{zz} E_{xy} E_{yx}) \\ &\quad - 8 (E_{xx} E_{yy} E_{zz} + E_{xy} E_{yz} E_{zx} + E_{xz} E_{zy} E_{yx}) \end{aligned} \quad (112)$$

$$p_4(E) = \det[M] = 2 \text{tr}[E \cdot E^t \cdot E \cdot E^t] - \left(\text{tr}[E \cdot E^t] \right)^2. \quad (113)$$

Interestingly, the polynomial $M(E)$ is arranged so that $-p_2(E)/2$ is the (squared) Fröbenius norm of E , and $-p_3(E)/8$ is its determinant. Our task now is to express the four eigenvalues $e = \epsilon_k(p_1, p_2, p_3, p_4)$, $k = 1, \dots, 4$, usefully in terms of the matrix elements, and also to find their eigenvectors; we are of course particularly interested in the maximal eigenvalue ϵ_{opt} .

Invariance. If we now write the sample matrix to explicitly show its derivation from the reference matrix, that is, $x_k^a = R(q)_{ab} y_k^b$ for all $k \in \{1, \dots, K\}$, then the cross-covariance matrix becomes

$$E_{ab} = \sum_{k=1}^N R(q)_{ac} [y_k]_c [y_k]_b = R(q)_{ac} [\mathbf{Y} \cdot \mathbf{Y}^t]_{cb}. \quad (114)$$

We now take the three distinct components of Eqs. (111), (112), and (113) and write them out as

$$\left\{ \begin{aligned} \det[E] &= \det \sum_k R_{ac} y_k^c y_k^a \\ &= \det R_{ac} \sum_k y_k^c y_k^a \\ &= \det E[Y, Y] \equiv \det E_0 \end{aligned} \right. \quad (115)$$

$$\left\{ \begin{aligned} \text{tr}[E \cdot E^t] &= \sum_{k,k'} R_{ac} y_k^c y_k^b R_{ad} y_{k'}^d y_{k'}^b \\ &= \sum_{k,k'} y_k^c y_k^b y_{k'}^c y_{k'}^b = \text{tr} E_0 \cdot E_0^t \end{aligned} \right. \quad (116)$$

$$\left\{ \begin{aligned} \text{tr}[E \cdot E^t \cdot E \cdot E^t] &= \text{tr}[E_0 \cdot E_0^t \cdot E_0 \cdot E_0^t] \end{aligned} \right. \quad (117)$$

Thus we know that, modulo assuming irrelevant errors in the data, the entire characteristic equation Eq. (109) is independent of the rotation matrix applied to obtain the sample data, and thus the eigenvalues of the profile matrix $M(E)$ are independent of the applied rotations embodied in the sample data; only the self-covariance of the reference data

$$E_0 = \mathbf{Y} \cdot \mathbf{Y}^t \quad (118)$$

enters into the determination of the eigenvalues of $M(E)$, and since E_0 is symmetric, the last three elements of the top row and left-hand column of $M(E_0)$ *vanish*, making the maximum eigenvalue just

$$[\text{max eigenvalue}](M(E_0)) = \text{tr}[E_0].$$

C The Adjugate Matrix

Standard methods for finding the rotation aligning a rotated 3D point cloud with its reference cloud (see, e.g., Horn, 1987; Hanson, 2020) determine the optimal quaternion by finding the maximal eigenvalue of a certain 4×4 matrix. The normalized eigenvector of that maximal eigenvalue is q_{opt} , the quaternion determining the optimal aligning rotation matrix $R_{\text{opt}} = R(q_{\text{opt}})$. Buried in the last step of this routine linear algebra calculation, we have in fact a mandatory process that closely parallels the complicated axis-angle procedure just described above. The key observation is that there is an ambiguity in the process of going from a symmetric real matrix M and one of its eigenvalues λ to a well-behaved corresponding eigenvector.

One needs a small piece of linear algebra to follow this train of thought. First, we recall that the determinant of a square real matrix can be computed using the *Adjugate Matrix* built from the transposed cofactors of the matrix. Dividing the Adjugate by the determinant itself yields the *inverse*, that is, if the matrix M is nonsingular, then

$$M^{-1} = \frac{\text{Adjugate}(M)}{\det M} \quad \rightarrow \quad M \cdot \text{Adjugate}(M) = \det M \, I_4 ,$$

where I_4 is the 4D identity matrix. Here we will be particularly interested in the special case where $\det M = 0$, so that the inverse does not exist. Nevertheless, the Adjugate matrix may *still exist* for singular matrices because it is completely linear:

$$\text{Adjugate}(M)_{ij} = \text{Transpose}(\text{Cofactor Matrix})(M_{ij}) \quad .$$

However, another step is needed to understand how we will exploit the Adjugate. All the matrices we will be examining will be real symmetric 4D matrices, so we there will exist a

characteristic equation with real eigenvalues λ depending on four polynomials of the set of matrix elements $\{m_{ij}\}$ of M , which takes the form

$$\begin{aligned} \det(M(m) - \lambda I_4) &= \lambda^4 + \lambda^3 p_1(m) + \lambda^2 p_2(m) + \lambda p_3(m) + p_4(m) \\ &= 0 . \end{aligned} \quad (119)$$

Here the $p_k(m)$ are polynomials of degree k in the matrix elements m . The characteristic equation Eq. (119) of M has four real roots, and in ordinary circumstances these are distinct, each has an eigenvector, and there is a unique “maximal” eigenvector corresponding to the largest eigenvalue, which we now denote by λ_{opt} . *By definition* substituting λ_{opt} into the characteristic equation solves the eigenvalue problem, so we may denote this special context of the characteristic equation by the matrix

$$\chi = [M - \lambda_{\text{opt}} I_4] ,$$

where χ itself is singular, $\det \chi \equiv 0$. Then the *Adjugate matrix* $A(M, \lambda)$ is defined as the transposed cofactor matrix of χ , constructed precisely so that each column of A produces the *determinant* $\det \chi$. Now, since the determinant of χ vanishes by construction, we can split the two terms in the definition of χ as follows:

$$\chi \cdot A = M \cdot A - \lambda A = \det \chi \equiv 0 .$$

Thus *all four columns* of the Adjugate A are in principle eigenvectors of the *same* λ_{opt} . The essential caveat is that if any of the rows or columns of the (symmetric) matrix A have a vanishing or very small norm, that eigenvector will be of little practical use, and a *different column* must be chosen as the eigenvector corresponding to λ_{opt} for further calculations. Typical linear algebra libraries perform these checks by default using a variety of methods; here, we will argue that, due to the nontrivial spherical manifold \mathbf{S}^3 on which quaternions live, one must explicitly take into account the properties of the *entire* Adjugate matrix as it appears in quaternion calculations that involve an explicit or implicit eigensystem. We show explicitly in the main text that typical contexts that extract quaternions from measured rotation matrices meet this criterion.

Summary of Results. Only the *Adjugate matrix* of a particular 4×4 matrix, written in terms of unnormalized quadratic pre-quaternion forms, can be expressed in a nonsingular fashion in terms of rotation matrix elements. If we simply set Eq. (1) equal to Eq. (2), $R(q) = R(\theta, \hat{\mathbf{n}})$, assuming that $R(\theta, \hat{\mathbf{n}})$ corresponds to an ideal noise-free measurement, we will construct a symmetric 4×4 matrix of algebraic expressions for all 10 quadratic quaternion terms that is, critically, square-root-free and division-free:

$$K(q) = \begin{bmatrix} q_0^2 & q_0 q_1 & q_0 q_2 & q_0 q_3 \\ q_0 q_1 & q_1^2 & q_1 q_2 & q_1 q_3 \\ q_0 q_2 & q_1 q_2 & q_2^2 & q_2 q_3 \\ q_0 q_3 & q_1 q_3 & q_2 q_3 & q_3^2 \end{bmatrix} = \frac{1}{2} \begin{bmatrix} 1+c & s \hat{n}_1 & s \hat{n}_2 & s \hat{n}_3 \\ s \hat{n}_1 & (1-c) \hat{n}_1^2 & (1-c) \hat{n}_1 \hat{n}_2 & (1-c) \hat{n}_1 \hat{n}_3 \\ s \hat{n}_2 & (1-c) \hat{n}_1 \hat{n}_2 & (1-c) \hat{n}_2^2 & (1-c) \hat{n}_2 \hat{n}_3 \\ s \hat{n}_3 & (1-c) \hat{n}_1 \hat{n}_3 & (1-c) \hat{n}_2 \hat{n}_3 & (1-c) \hat{n}_3^2 \end{bmatrix} . \quad (120)$$

Note that, in the exact case, the quaternion origins of the polynomials in $K(0)$ imply the existence of nontrivial constraints. For the situation of inexact rotation data $R(m)$ replacing $R(\theta, \hat{\mathbf{n}})$, similar expressions hold with the same qualitative features.

In all cases, each row (or column) of the measured data on the right-hand side corresponds to a full 4-element quaternion *scaled* by a factor of q_0 , q_1 , q_2 , or q_3 as the only type of object that can be reliably expressed without encountering normalization singularities. These can be removed by simple normalization *if* the normalizing divisor is not too near the floating point precision limit for zero. There are in fact 14 different sets of singular quaternion submanifolds, corresponding topologically to the 4 vertices, 6 edges, and 4 faces of an abstract tetrahedron, that is, quaternions with zeroes in three, two, or one of their four elements. The constraint $q \cdot q = 1$ guarantees that *at least one row* of Eq. (120) can always be normalized to produce a valid quaternion q_{opt} and its pure rotation matrix $R(q_{\text{opt}})$ that is the best approximation to the numerically measured matrix $R(\theta, \hat{\mathbf{n}})$ or $R(m)$. The algorithm is, not surprisingly, very close to the classic algorithm of Shepperd (1978): find the row whose diagonal element is the largest, and normalize that row to find a quaternion q_{opt} . This is also similar, but not identical, to the Ansatz of Xiang and Li (2020), which achieves a non-singular result heuristically without our more complete theoretical underpinnings.

D The Fourteen Adjugate Matrices Exhibiting Unnormalizable Quaternion Geometry

Strategy for depicting the full quaternion map. Despite its four-dimensional intrinsic nature, quaternion geometry can be depicted in a fairly accurate way if we are willing to follow some analogies between lower dimensional and higher dimensional spheres. First, we show in Fig. (8)(a) an ordinary sphere \mathbf{S}^2 embedded in 3D Euclidean space \mathbb{R}^3 , with the three orthogonal axes \hat{x} , \hat{y} , and \hat{z} , projected in the familiar way to a 2D image. Even though the image is a dimension lower than the actual 3D object being depicted, we are accustomed to interpreting this image as a 3D object. Now rotate the sphere as in in Fig. (8)(b) so that the three axes are projected equally onto the 2D image, with the ends of the axes forming the vertices of an equilateral triangle. Now we see that this projection corresponds to one hemisphere of \mathbf{S}^2 flattened into a disk containing all three positive axes, and the back hemisphere as a second disk containing all three negative axes. It is clear that if we create two separate images as in Fig. (8)(c,d), *every single point* on the manifold \mathbf{S}^2 can be seen in the two separate hemispherical images. We can do the same thing with a full quaternion map using a *solid ball* containing a 3D quadruple of positive axes (with the four axis ends being the vertices of a tetrahedron), paired with a matching solid ball containing the symmetric projections of the four negative axes. Every point of the quaternion sphere is visible in the two solid balls, exactly analogous to the two filled disks for the hemispheres of \mathbf{S}^2 in Fig. (8)(c).

The full quaternion map from the unnormalized representation to the normalized true quaternion sector is divided into eight distinct regions, in opposite signed pairs that represent equivalent rotations due to the identification $R(q) = R(-q)$. Instead of portions of ordinary spheres as in the top of Figure 3, we have portions of hyperpheres centered at $(\pm 1, 0, 0, 0)$, $(0, \pm 1, 0, 0)$, $(0, 0, \pm 1, 0)$, and $(0, 0, 0, \pm 1)$. Instead of being partial hemispherical surfaces, these are now solid balls, each corresponding to a portion of a set of overlapping hemispheres of the quaternion manifold \mathbf{S}^3 . These are difficult to draw, but an attempt can be made by projecting the axes of the 4D space into 3D in the symmetric directions of the vertices of a tetrahedron. In Figure 9(a), we show first a collection of slices of the solid ball at various radii in 4D, aligned with one axis, for a single choice of the eight unnormalized and normalized maps. Then in Figure 9(b), we reduce the number of samples of the solid balls to one, but show a representative pair of unnormalized and normalized slices for *the four positive unit 4D axes*; there is another opposite sign counterpart for each of these four that is omitted for clarity.

Perhaps another useful way to look at the algebraic implications of quaternion adjugate normalization anomalies is simply to write down the fourteen $[q_\mu q_\nu]$ matrices that result for any combination of single, double, and triple choices of indices for the q_k from the set

$k \in \{0, 1, 2, 3\}$. For the four point pairs, with any three zeroes chosen, there are no degrees of freedom left, only identity quaternions; for the six with two zeroes chosen, there is a circle lying on $x^2 + y^2 = 1$, while for the four remaining singularities, there is a sphere \mathbf{S}^2 described by the constraint $x^2 + y^2 + z^2 = 1$. The matrices here are essentially the algebraic version of the graphics in Fig. (3):

$$\begin{array}{cccc}
123: \begin{bmatrix} \pm 1 & 0 & 0 & 0 \\ 0 & 0 & 0 & 0 \\ 0 & 0 & 0 & 0 \\ 0 & 0 & 0 & 0 \end{bmatrix} & 023: \begin{bmatrix} 0 & 0 & 0 & 0 \\ 0 & \pm 1 & 0 & 0 \\ 0 & 0 & 0 & 0 \\ 0 & 0 & 0 & 0 \end{bmatrix} & 013: \begin{bmatrix} 0 & 0 & 0 & 0 \\ 0 & 0 & 0 & 0 \\ 0 & 0 & \pm 1 & 0 \\ 0 & 0 & 0 & 0 \end{bmatrix} & 012: \begin{bmatrix} 0 & 0 & 0 & 0 \\ 0 & 0 & 0 & 0 \\ 0 & 0 & 0 & 0 \\ 0 & 0 & 0 & \pm 1 \end{bmatrix} \\
01: \begin{bmatrix} 0 & 0 & 0 & 0 \\ 0 & 0 & 0 & 0 \\ 0 & 0 & x & y \\ 0 & 0 & y & x \end{bmatrix} & 02: \begin{bmatrix} 0 & 0 & 0 & 0 \\ 0 & x & 0 & y \\ 0 & 0 & 0 & 0 \\ 0 & y & 0 & x \end{bmatrix} & 03: \begin{bmatrix} 0 & 0 & 0 & 0 \\ 0 & x & y & 0 \\ 0 & y & x & 0 \\ 0 & 0 & 0 & 0 \end{bmatrix} & \\
23: \begin{bmatrix} x & y & 0 & 0 \\ y & x & 0 & 0 \\ 0 & 0 & 0 & 0 \\ 0 & 0 & 0 & 0 \end{bmatrix} & 31: \begin{bmatrix} x & 0 & y & 0 \\ 0 & 0 & 0 & 0 \\ y & 0 & x & 0 \\ 0 & 0 & 0 & 0 \end{bmatrix} & 12: \begin{bmatrix} x & 0 & 0 & y \\ 0 & 0 & 0 & 0 \\ 0 & 0 & 0 & 0 \\ y & 0 & 0 & x \end{bmatrix} & \\
0: \begin{bmatrix} 0 & 0 & 0 & 0 \\ 0 & x & y & z \\ 0 & z & x & y \\ 0 & y & z & x \end{bmatrix} & 1: \begin{bmatrix} x & 0 & y & z \\ 0 & 0 & 0 & 0 \\ z & 0 & x & y \\ y & 0 & z & x \end{bmatrix} & 2: \begin{bmatrix} x & y & 0 & z \\ z & x & 0 & y \\ 0 & 0 & 0 & 0 \\ y & z & 0 & x \end{bmatrix} & 3: \begin{bmatrix} x & y & z & 0 \\ z & x & y & 0 \\ y & z & x & 0 \\ 0 & 0 & 0 & 0 \end{bmatrix} \\
& & & (121)
\end{array}$$

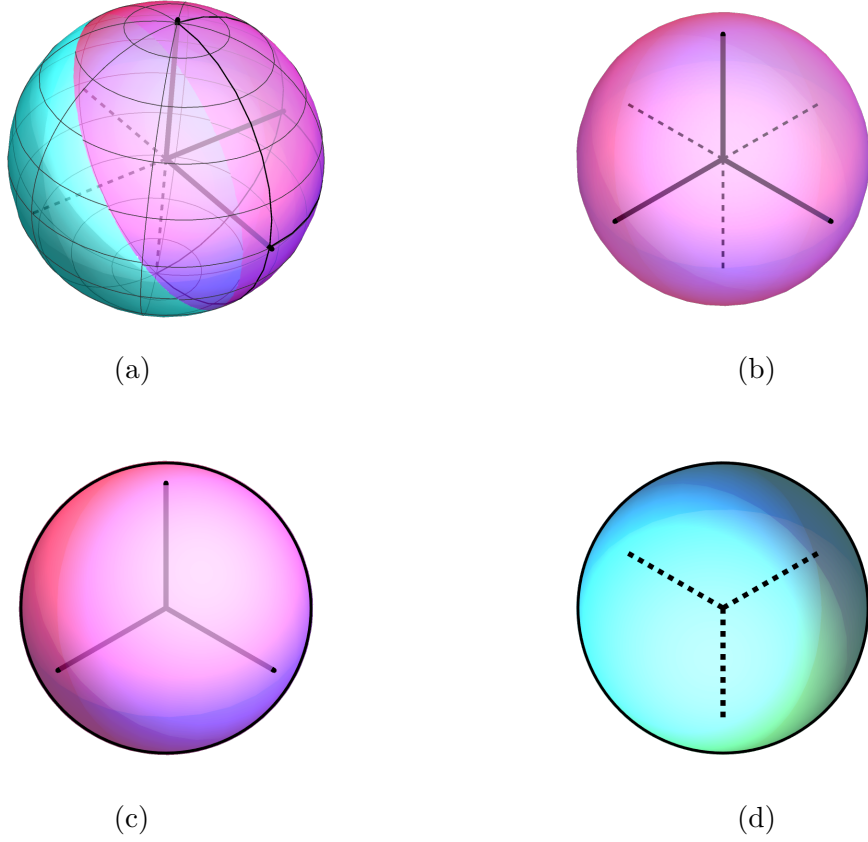


Figure 8: **Analog of S^3 projection with the S^2 full and hemispherical projection..** (a) The two-sphere S^2 contains three orthogonal axes in its 3D-space projection, shown obliquely here to expose the positive (solid) and negative (dashed) ends of the coordinate axes using a general viewpoint. (b) If we look straight down the diagonal, the three axes, both positive and negative ends of the axes appear in the 2D image to be the vertices of an equilateral triangle. (c,d) If we simply display the 2D disk with the positive axes in a planar image separately from the 2D disk with the negative axes, we can see a (flattened) depiction in which *every single point* of S^2 is visible and distinct. In order to make every single point of the quaternion hypersphere S^3 visible in our images, we will simply put the *four* axes of 4D space at the symmetrical vertices of a tetrahedron, and use a pair of solid balls (simulating 3D space of course using 3D graphics images) instead of a pair of filled disks.

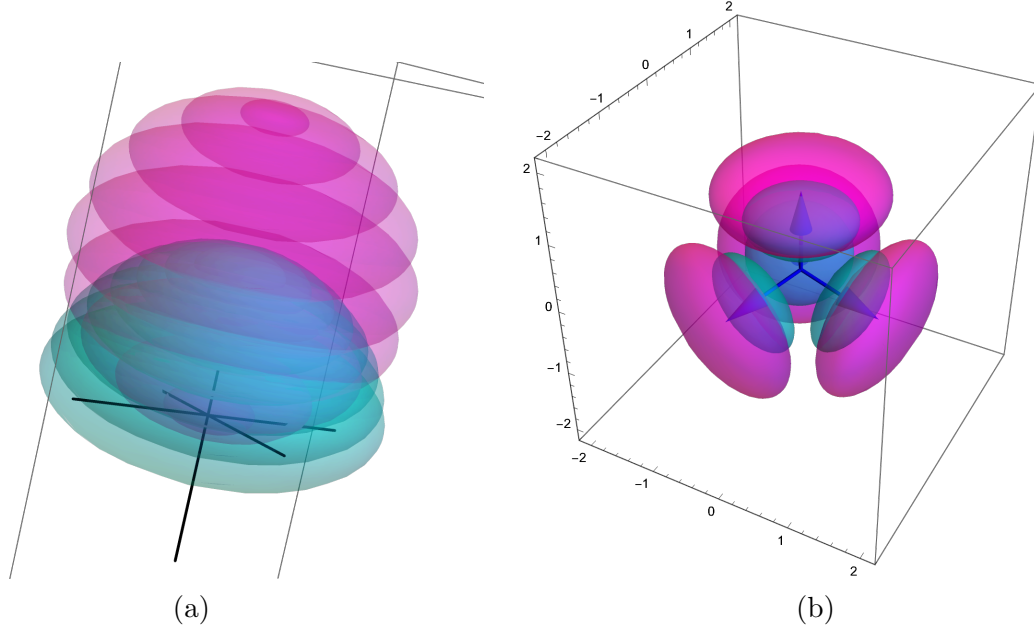


Figure 9: 3D subspace showing three axes of singularities. In this 3D subspace of quaternion space, there are partial spheres instead of partial circles, but the singularity occurs in the same way, as the sphere closes in on the origin, normalization is impossible. The four axes correspond to the q_0 , q_1 , q_2 , and q_3 quaternion directions projected down symmetrically to the directions of the four vertices of a 3D regular tetrahedron. While there are 8 actual axes in 4 pairs, corresponding to the two pairs of axes $x = \pm 1$ and $y = \pm 1$ in Fig. (2), here for readability we can only show the four positive axes directions whose manifold patches cover the solid ball that is the “Northern hemisphere” of \mathbf{S}^3 ; the unshown “Southern hemisphere” is the second solid ball that, sewn onto the Northern hemisphere along the \mathbf{S}^2 equator, completes the full \mathbf{S}^3 manifold. (a) A single pair of solid-ball patches, the larger corresponding to the $+q_0$ direction of the solution space q_0 (q_0, q_1, q_2, q_3); the smaller ball is the normalized version collapsing to a patch on the actual \mathbf{S}^3 patch that normalizes without singularity in the neighborhood of $q_0 \approx +1$. (b) The four pairs that cover the nonsingular patches around $q_0 \approx +1$, $q_1 \approx +1$, $q_2 \approx +1$, and $q_3 \approx +1$. The actual mathematical balls correspond to a volume rendered solid, which is difficult to portray in a figure, so multiple level sets are shown for each ball to depict the continuous volume with a finite sampling of spherical surfaces.

E Proposed Solution Procedure For Perspective

Proposed Solution Procedure For Perspective. Without making any claims to an optimal solution, we proceed to describe a *reasonable* three-step procedure following the concepts laid out in Section 5.4:

- **Find the best orthographic approximation to the needed rotation.** From the assumed input point-cloud data $\{\mathbf{x}_k\}$ and the matched image-plane data $\{\mathbf{u}_k\}$, we can calculate from Eq. (95) a good approximation to the needed rotation \tilde{R} that is very accurate at the center of the projected image, and is disturbed by the growing perspective projection distortion for points farther from the projection center. In many cases, this approximation itself will already be quite good.
- **Optimize \tilde{R} .** However, as before, due to the errors being introduced relative to a perfect orthographic data set (in this case compounded by perspective distortion), \tilde{R} will not in general be an actual rotation; we proceed again to apply the Bar-Itzhack optimization as in section 5.4 to produce a quaternion q_{opt} that corresponds to the *optimal* pure rotation matrix $R_{\text{opt}} = R(q_{\text{opt}})$ closest to the imperfect \tilde{R} .
- **Define the focal-length determination as a separate optimization step.** If we want to provide an estimate for the camera position via the focal length, we can add a final step to the procedure by simply inserting the now-constant matrix

$$R_{\text{opt}} = \begin{bmatrix} P(q_{\text{opt}}) \\ D(q_{\text{opt}}) \end{bmatrix}$$

into Eq. (102). This now becomes a loss function $\mathbf{S}(\bar{f})$ depending *only* on the inverse focal length \bar{f} , or $\mathbf{S}(f)$ depending *only* on the focal length f . Upon differentiation with respect to \bar{f} , the first context results in an equation whose numerator is a polynomial of order $(3K - 2)$, and can easily be solved numerically to give \bar{f} . The alternative using $\mathbf{S}(f)$ results in the explicit solution Eq. (104) for f .

There also appears to be no obstacle to using this as an improved starting point for iterative refinement schemes such as Lu et al. (2000).